Using the Hα Spectral Line to Isolate the Oldest Galaxies at $0.05 < z < 0.15$

Willy D. Kranz

Zurich, August 18, 2009
Institute for Theoretical Physics, University of Zurich

Master-Thesis under the supervision of Prof. Dr. Kim-Vy Tran

Abstract

This work investigates the quality of a Hα-Balmer line as selection criterion for stellar old red sequence galaxies. Combined data from the SDSS DR6 and the NYU VAGC galaxy catalogues are used to construct a galaxy sample of $\sim$ 185,000 objects at $0.05 < z \leq 0.15$. Using that we select 3 red sequence samples by applying 3 different selection criteria; 1) the equivalent width of Hα, 2) the Sérsic index n and 3) the galaxy colour $(g' - r')$. Colour-magnitude evaluation, BPT-emission line diagnostics (Baldwin *et al.* 1981 [2]) and the analysis of photometric and spectroscopic indices allow us to determine the composition of each red sequence sample in detail.
We demonstrate that the Hα criterion selects the tightest red sequence having only a colour residual scatter of $\sigma_{\rm MAD} \sim 0.05$, that is half the scatter value of the morphology (Sérsic index) selected red sequence where $\sigma_{\rm MAD}$ is ~ 0.1. We show also that the Hα selected red sequence consists only of passive galaxies and that a morphology selected sample features a fraction of at least 12.6% star forming and AGN galaxies. We show further, that additional colour information can maximal reduce this fraction of emission line galaxies to only 4%.
For each red sequence sample we construct a luminosity weighted average spectrum, measure its D4000 flux ratio and use that to calculate each sample's average stellar age. We find that the Hα selected galaxy sample has an average D4000 value of ~ 1.77 and an average stellar age of about 4 Gyr. Due to the inclusion of star forming/AGN objects the other two red sequence samples (Sérsic and colour selected) feature significantly lower D4000 means and show average stellar ages between 2.6 - 3.2 Gyr. We check these sample ages for redshift dependence and find that the Hα spectral line is the most reliable indicator of stellar old systems at any $z \leq 0.15$.
We demonstrate that the single Hα spectral index features strong correlations with galaxy colour $(g' - r')$, Sérsic index and other spectral indices, like the 4000Å-break or the O[II]-line, and conclude that Hα-line is the best selection criterion to pick a homogeneous old galaxy sample of early-type red sequence galaxies. Using our Hα-selected pure sample of stellar old galaxies enable us to study the average characteristics of the Universe's most stellar aged systems in a more cleaner way than before.

Acknowledgment

I would like to thank Lea Giordano, Dr. Amélie Saintonge and Prof. Dr. Kim-Vy Tran for making all this possible. Their guidance, help and motivation influenced and improved this work significantly.

Contents

Chapter 1

Introduction

How did early-type galaxies form and how did they evolve after that. These two important questions of galaxy evolution cannot completely answered today. The most common way to analyse galaxy evolution is to look into the colour-magnitude diagram of early-type galaxies. It is known that early-type galaxies are redder, more massive & luminous than late-type systems and that early-type galaxies form the red sequence in colour-magnitude space obeying a colour-magnitude relation (CMR) over at least 4 magnitudes (Baum 1959 [3], Visvanathan & Sandage 1977 [51], Sandage & Visvanathan1978 [44], Bower *et al.* 1992 [9]). The CMR shows redder colours at higher luminosities, a result arising from the fact that stellar age & metallicity of early-type systems are changing along the red sequence so that brighter objects feature higher stellar ages & higher metallicities (Faber 1973 [19], Worthey *et al.* 1994 [53]). Metallicity & stellar age are degenerated quantities, therefore it is not directly clear which parameter is the main driver of the CMR's slope. However, the works of Faber 1973 [19], Bower *et al.* 1992 [10], Kauffmann & Charlot 1998 [33], and the recent studies of Gallazzi *et al.* 2006 [25], Graves *et al.* 2007 [28] & 2009 [27] suggest that rather the increase in metallicity than an increase in stellar age at higher luminosities causes the redder colours of the CMR. Nevertheless, the stellar age of red sequence members should not be neglected if one wants to explain the CMR slope of the early-type systems (Faber *et al.* 1995 [20], Ferreras *et al.* 1999 [21]).

Looking into the evolution of the red sequence, Ellis *et al.* 1997 [18] showed that the CMR slope does not change up to $z \sim 1$. Their result is based on the passive galaxy evolution of clustered early-type systems. These galaxies formed the majority of their stars at $z > 2$ and evolve only passively after that. Bell *et al.* 2004 [4] on the other hand found in their morphology selected red sequence sample a stronger CMR evolution taking place from $z = 0$ to $z \sim 1$. Their sample of early-type red sequence galaxies based on COMBO-17 photometry data showed bluer rest frame colours at higher redshifts, a clear hint of evolutionary changes in the stellar population of red sequence objects. However, Bell *et al.* 2004 [4] confirmed also that the majority of stars of early-type red sequence galaxies was formed at $z > 2$.

Today, there are in general two scenarios explaining the evolution of the red sequence by looking into the formation of early-type galaxies, their arriving on the red sequence and how they settle & evolve on the red sequence after that. The monolithic formation scenario says that early-type objects are formed in dense environments early in time ($z > 2$), featuring a star formation burst, and after that settle on the red sequence early due to passive galaxy evolution (Ellis *et al.* 1997 [18], Thomas *et al.* 2005 [50]). In this scenario the hot & dense environments around early-type galaxies prevent any new occurring star formation activity and the most massive & luminous early-type objects are formed via dry merging of less massive ellipticals. Even during these merging process the passive galaxy evolution will remain intact. Following this scenario we should find many less massive non-star forming early-type objects on the red sequence at redshifts $z \sim 2$. Furthermore, the galaxy mass on the red sequence and the slope of the CMR should stay nearly constant through time since $z \sim 2$. The other, hierarchical scenario of galaxy formation says that massive early-type systems are formed later in time by merging of less massive disk galaxies. The emerged galaxy arrives then on the red sequence due to the merging-based truncation of star formation (Kauffmann & Charlot 1998 [33]). It is believed that AGN-feedback is mainly responsible for ending star formation in these merging galaxies (Bower *et al.* 2006 [8], Croton *et al.* 2006 [14]). Unlike the monolithic scenario, the hierarchical merging mechanism predicts larger changes of the CMR slope at higher redshifts due to the decrease of red sequence members. It forcasts fewer less massive non-star forming early-type galaxies on the red sequence and more blue starforming late-type systems off the red sequence at higher z. Therefore, one expects also that the galaxy mass on the red sequence decreases with increasing redshift. In this scenario the galaxy mass on the red sequence is not as constant in redshift space than it is in the monolithic formation scenario.

To determine which formation scenario of early-type galaxies dominates the assembly of the red sequence and to see how the red sequence and its CMR evolve through time, it is necessary and essential to reliably identify early-type red sequence galaxies at any redshifts. Selecting red sequence members by early-type morphology (Sandage 1961 [43]), or the surface brightness profiles of early-type objects (de Vaucouleurs 1948 [15], Sérsic 1963 [46]), is not easy to accomplish at higher redshifts. The galaxy resolution decreases with z, especially for ground based telescopes where turbulences in the Earth's atmosphere reduce the galaxy's resolution even further. It is also known that determining star formation rates or stellar ages from galaxy colours is not always reliable, judging by colour can mislead to wrong results, especially if one looks at dusty galaxies. With spectroscopy we can overcome these disadvantages. The Balmer spectral lines are reliable tracer of galaxy's current star formation rate, and it is also known that the early-type galaxies of the local Universe ($z < 0.3$) show Balmer-line absorption in their spectra due to their passive evolution (Dressler & Gunn 1983 [17], Kennicutt 1998 [37], Yan *et al.* 2004 [54]).

We show in this work that selecting by Hα-absorption alone will provide one with a pure

sample of non-star forming & stellar old early-type red sequence galaxies. We will demonstrate that the Hα line is a better and more reliable indicator of stellar old red sequence galaxies than the photometric criteria of morphology and/or colour and that the Hα absorption criterion selects only early-type galaxies with Sérsic $n \geq 2$. The recent and huge galaxy catalogs of the Sloan Digital Sky Survey Data Release 6 (SDSS DR6; Stoughton *et al.* 2002 [48], Adelman-McCarthy *et al.* 2008 [1]) and the NYU Value-Added Galaxy Catalog (NYU VAGC; Blanton *et al.* 2005 [7]) allow us to select 3 different red sequence samples by using 2 photometric & 1 spectroscopic selection criteria. With these red sequence samples and the variety of measured galaxy parameters listed in the SDSS DR6 & NYU VAGC catalogues we are able to reliably explore the selection effects of our applied criteria in different parameter spaces. In this manner we can show that the Hα criterion selects the most homogeneous and pure sample of stellar old & non-star forming early-type red sequence galaxies independent of redshift, and that the criteria of galaxy colour & morphology are less effective in this task. Using the Hα criteria at higher redshifts ($z > 2$) should then enable us to determine in a more detailed and accurate way compared to before (see references above) at which z the first non-star forming early-type galaxies arrived on the red sequence and how the mass assembly of the red sequence progressed further in time (red sequence evolution and the z dependent changes of the CMR). Having a individual spectrum of each Hα-passive red sequence galaxy should allow us to calculate stellar ages & metallicities along the red sequence at different redshifts. This could provide us with new insights about age/metallicity degeneracy of the red sequence and how this affects the slope of the CMR through time.
In Section 2 we present the used data and describe the applied selection criteria. The results of our different red sequence selections are shown in Section 3 and are discussed in Section 4. Our conclusions can be found in Section 5. We use concordance Cosmology with $\Omega_0 = 0.3$, $\Omega_\Lambda = 0.7$, $H_0 = 100\ h$ km s^{-1} Mpc^{-1}, $h = 1$ in this work.

Chapter 2

Data

In this work we use spectroscopic data from the Sloan Digital Sky Survey (SDSS), Data Release 6 (DR6)[a] (Stoughton *et al.* 2002 [48], Adelman-McCarthy *et al.* 2008 [1]) and photometric data from the NYU Value-Added Galaxy Catalog (NYU VAGC)[b]. The main galaxy sample of the SDSS DR 6 includes more than 790,000 galaxy spectra and provides one with a variety of measured spectral indices, *e.g.* the D4000-value (flux ratio of the 4000Å-break) and the equivalent widths (EWs) of Hα, Hβ and O[III] (Adelman-McCarthy *et al.* 2008 [1]). The NYU VAGC supplements the SDSS measurements with additional data that includes the galaxy's extinction corrected Petrosian magnitude, Sérsic index n, and the K-corrected absolute magnitude. The combined use of both catalogs enables us to explore the diversity of these parameters for a statistically large number of galaxies.

2.1 SDSS

2.1.1 DR6 Galaxy Catalog

The Sloan Digital Sky Survey (SDSS) is an optical survey using the 2.5 m telescope at the Apache Point Observatory in New Mexico (USA). SDSS uses 5 filter bands for its photometry: $u'g'r'i'z'$ (Fukugita *et al.* 1996 [24], Stoughton *et al.* 2002 [48]). The SDSS also includes spectroscopic observations with a wavelength range coverage of λ = 3800Å - 9200Å at a resolution of $\sim$ 2.7Å/pixel. From the SDSS, we use the measured equivalent widths (EW) of Hα, Hβ, N[II] λ6585 and O[III] λ5007; negative EWs denote absorption lines.
We also use the 4000Å-break as measured by the D4000 flux ratio value. SDSS uses the D4000 bandpass definitions of Bruzual 1983 [11] and calculates the D4000 flux ratio with $f_{\rm blue}/f_{\rm red}$, where $f_{\rm blue}$ is the flux in the 3750Å-3950Å bandpass and $f_{\rm red}$ the flux in the 4050Å-4250Å bandpass. This flux ratio results in a D4000 value of less than one for nearly

[a] see web page: http://www.sdss.org/dr6/index.html
[b] see web page: http://sdss.physics.nyu.edu/vagc/

all galaxies inside the SDSS catalogue. To make the D4000 flux ratio comparable to the work of others, *e.g.* Kauffmann *et al.* 2003 [36] and Gonzalez-Delgado *et al.* 2005 [26], we use the inverse of the SDSS D4000 value ($1/\mathrm{D4000_{SDSS}}$ = D4000 herein). However, note that this D4000 value differs from the narrow band flux ratio $\mathrm{D_n4000}$ used by Kauffmann *et al.* 2003 [36] and Gonzalez-Delgado *et al.* 2005 [26] in terms of band definitions. The D4000 value measured by SDSS uses a bandpass $\triangle\lambda = 200$Å and is thus more susceptible to metallicity effects than the $\mathrm{D_n4000}$ flux ratio (because it uses narrower bandpasses, $\mathrm{D_n4000}$ contains fewer Fe-lines).

2.1.2 NYU Value-Added Galaxy Catalog

The NYU Value-Added Galaxy Catalog (NYU VAGC) is based on the SDSS DR6 catalog and provides additional photometric parameters (Blanton *et al.* 2005 [7]). The authors of the NYU VAGC boosted the apparent "extinction-corrected Petrosian magnitude limit" (Blanton *et al.* 2005 [7]) for galaxies to $r' = 18$ (apparent magnitude of r'-band). The extinction correction was determined from the dust maps of Schlegel *et al.* 1998 [45].
The NYU VAGC includes the values of Sérsic index n (see Sérsic 1968 [47]) and absolute magnitude M in all five filter bands ($u'g'r'i'z'$) for nearly all SDSS DR6 galaxies. The K-corrected absolute magnitude M in each filter band has been computed via

$$M_f = m_f - 5\,\log_{10}\left[D_L/10\mathrm{pc}\right] - K_f(z), \tag{2.1.1}$$

where D_L is the luminosity distance and m_f the apparent magnitude of filter band f (in our case r'). In the catalog, the K-corrections $K_f(z)$ were calculated for each galaxy individually with Blanton's `kcorrect` software version v4_1_4 (Blanton & Roweis 2007 [6]; Hogg *et al.* 2002 [30]).
In this work we will use the NYU VAGC's apparent Petrosian magnitudes g' & r' (magnitudes named after the g'- & r' filter bands), the Sérsic index n as measured in the r'-filter band, and the absolute Petrosian magnitude $M_{r'}$ (also measured in the r'-filter band). The NYU VAGC also includes an estimator of the galaxy's metallicity that we will use in part of our analysis.

2.2 Main Galaxy Sample

Our Main Galaxy sample (MG) includes only galaxies with $0.05 < z \leq 0.15$. The low redshift cut of $z = 0.05$ is necessary to avoid aperture problems due to the $3''$ diameter size of the spectroscopic fibers: at $z < 0.05$ the SDSS spectra tend to only include light from the central regions of the galaxies. The high redshift cutoff of $z = 0.15$ provides a magnitude range of at least 1.5 magnitudes in a complete sample even at at the higher redshift end.

We use an apparent magnitude limit of $r' < 17.7$ (apparent magnitude of the r'-band) in our Main Galaxy sample which is comparable to the limits of $r' < 17.77$ and $r' < 18$ in the SDSS DR6 catalogue and the NYU VAGC, respectively (Gunn *et al.* 1998 [29], York *et al.* 2000 [56], Strauss *et al.* 2002 [49], Blanton *et al.* 2005 [7]). Our magnitude limit provides a reliably complete galaxy sample from the combined catalogues.
The galaxies in our Main Galaxy sample are required to have:

1. a median signal-to-noise ratio > 3 in the g'- and r'-band photometry
2. a median (S/N) > 5 over the entire spectrum
3. a measured (S/N) > 2 in the Hα line

Furthermore, each galaxy must have an absolute Petrosian r'-band magnitude $M_{r'}$ brighter than the K-corrected completeness limit of

$$M_{r',limit} = 17.7 - 5\,\log_{10}\left[D_L/10\mathrm{pc}\right] - K_{ave}(z) \tag{2.2.2}$$

where D_L is the luminosity distance, 17.7 is our applied apparent r' magnitude limit, and $K_{ave}(z)$ is the average K-correction determined using:

$$K_{ave}(z) = 1.2106z - 0.0104 \tag{2.2.3}$$

The average K-correction shown in Eq. 2.2.3 is based on the r'-band K-corrections of Hα absorption-line galaxies in the NYU VAGC. Earlier work by Quintero *et al.* 2004 [42] showed that galaxies with Hα absorption have an early-type spectral energy distribution (SED) and thus there is little scatter in their r'-band K-correction with redshift in the redshift range of our study ($0.05 < z \leq 0.15$). A σ-clipped linear least squares fit to the Hα absorption-line galaxies gives Eq. 2.2.3 with a 3σ deviation of less than 0.02 mag; note that this relation is valid only for passive galaxies.
The Main Galaxy sample is split into 20 redshift bins of width $\triangle z = 0.005$. The effects of passive galaxy evolution and assuming an SED to determine K-corrections on colours and magnitudes are negligible within such narrow redshift bins. Each redshift bin's limiting absolute Petrosian magnitude is set at the the upper z value. Table 2.1 lists the 20 redshift bins with their $\triangle z$ ranges, limiting absolute magnitude in $M_{r'}$, and the number of galaxies N_{gal} that meet all our selection criteria.

Table 2.1: *The Main Galaxy (MG) Sample*

$\triangle z$	N_{gal}	$M_{r'}$ [a]
$0.050 < z \leq 0.055$	13,299	-18.5
$0.055 < z \leq 0.060$	12,424	-18.7
$0.060 < z \leq 0.065$	16,127	-18.9
$0.065 < z \leq 0.070$	16,365	-19.1
$0.070 < z \leq 0.075$	18,992	-19.3
$0.075 < z \leq 0.080$	19,625	-19.4
$0.080 < z \leq 0.085$	19,861	-19.6
$0.085 < z \leq 0.090$	16,900	-19.7
$0.090 < z \leq 0.095$	14,439	-19.8
$0.095 < z \leq 0.100$	14,252	-20.0
$0.100 < z \leq 0.105$	13,473	-20.1
$0.105 < z \leq 0.110$	13,356	-20.2
$0.110 < z \leq 0.115$	14,334	-20.3
$0.115 < z \leq 0.120$	13,327	-20.4
$0.120 < z \leq 0.125$	11,698	-20.5
$0.125 < z \leq 0.130$	11,936	-20.6
$0.130 < z \leq 0.135$	12,120	-20.7
$0.135 < z \leq 0.140$	10,856	-20.8
$0.140 < z \leq 0.145$	9,362	-20.9
$0.145 < z \leq 0.150$	8,733	-21.0

[a] The applied r'-band absolute Petrosian magnitude cuts of each redshift bin. This absolute magnitude includes a K-correction for a "typical" Hα passive galaxy (early-type SED). These values are drawn as green solid lines in Figure 2.1.

2.2.1 MG1: Selecting with Hα

The Hα spectral line is the most reliable tracer of star formation in the optical spectrum (Kennicutt 1998 [37]; Yan *et al.* 2006 [55]): starforming galaxies have significant Hα emission, and Hα is not strongly affected by, *e.g.* dust. We use Hα to separate starforming and non-starforming galaxies and define our first Main Galaxy (MG1) sample to have galaxies with EW(Hα) < 0Å (Table 2.2).

Previous studies have used both Hα and [OII] to identify "quiescent" galaxies (Graves *et al.* 2009 [27], Yan *et al.* 2006 [55]) and shown that this population forms a tight colour-magnitude relation (CMR). However, [OII] can be strongly dust-extincted and is known to be an unreliable tracer of star formation (Jansen *et al.* 2001 [32], Yan *et al.* 2006 [55], Moustakas *et al.* 2006 [41]). Also, measurements of [OII] in galaxies at $z < 0.06$ with ground-based observatories is problematic due to absorption at λ <4000Åby the Earth's atmosphere. Our goal is to determine whether Hα alone can identify a uniformly old galaxy population.

Table 2.2: *Selection Criteria for the Main Galaxy (MG) Sample*[a]

Sample	Selection	EW Hα	Sérsic n	colour-cut
MG1	Hα	< 0	...	...
MG2	Sérsic	...	> 2	...
MG3	Sérsic + colour-cut	...	> 2	$3\sigma_{\rm MAD}$ of CMR

[a] All galaxies included in these samples have signal-to-noise ratios $\langle {\rm S/N} \rangle_{g'} > 3$, $\langle {\rm S/N} \rangle_{r'} > 3$, $\langle {\rm S/N} \rangle_{spec} > 5$, and $({\rm S/N})_{{\rm H}\alpha} > 2$. The $3\sigma_{\rm MAD}$ colour-cut is based on MG1's CMR and its colour residuals $\triangle(g' - r')$. MG1, MG2, and MG3 feature a variable completeness cut in $M_{r'}$ only valid for their narrow redshift range of $\triangle z = 0.005$ (see Table 2.1 & Figure 2.1).

2.2.2 MG2 & MG3: Selecting with Sérsic index & Colour

The Sérsic index n is used as a quantitative measure of a galaxy's morphology and is determined by fitting the axisymmetric surface brightness profile $I(r) = A\exp\left[-(r/r_0)^{1/n}\right]$ to a galaxy's surface brightness profile (Sérsic 1968 [47]). Galaxies with high Sérsic indices ($n > 2$) tend to be bulge-dominated (early-type) systems and those with lower indices ($n < 2$) to be disk-dominated (late-type) systems. The Sérsic index n depends strongly on the filter because a galaxy's surface brightness profile varies with observed wavelength. We use the Sérsic index measured in the r'-band from the NYU VAGC because r' is the most sensitive of the SDSS filters. We note that due to small errors in the measurement of the local sky level, there is a bias of $\sim (-0.5)$ in the computed Sérsic index such that a Sérsic index of $n \sim 3.5$ is measured for a real de Vaucouleurs surface brightness profile (Blanton *et al.* 2005 [7], Blanton *et al.* 2005 [5]).
Multiple studies use morphology and in particular Sérsic $n > 2$ to identify red sequence galaxies, *e.g.* Hogg *et al.* 2004 [31]. However, this does not provide a pure sample of red sequence galaxies: while the sample features a strong CMR, it also includes a large fraction of blue galaxies. For comparison to our Hα-selected (MG1) sample, we follow Hogg *et al.* 2004 [31] and select galaxies using Sérsic $n > 2$ for our second Main Galaxy (MG2) sample (see Table 2.2).
For a more refined comparison sample, we apply an additional color selection based on the scatter in the CMR of the Hα-selected (MG1) sample: our third Main Galaxy (MG3) sample thus includes both a selection on morphology (Sérsic $n > 2$) and color (Table 2.2). We use only galaxies with $\triangle(g' - r') > (-3\sigma_{MAD})$; because the color distribution is asymmetric, the median absolute deviation (MAD) is more appropriate for measuring the color scatter. A more extensive discussion of the color selection is in Section 3.1.

2.3 Luminous Galaxy Sample

In our analysis, we test the results from the Main Galaxy sample by comparing them to a Luminous Galaxy (LG) sample where we include all the galaxies at $0.05 < z \leq 0.15$ and apply an absolute magnitude limit of $M_{r'}$ = -21.0 (82,171 galaxies; see Fig. 2.1). Because the LG sample spans a wide redshift range, we use the K-corrected rest-frame magnitudes and colours from the NYU VAGC. Apply the same selection criteria as in the Main Galaxy sample, we have LG1 (EW Hα < 0Å), LG2 (Sérsic $n > 2$), and LG3 (Sérsic $n > 2$ & color-cut). Table 2.3 lists the criteria for these three samples and how many galaxies are in each.

Table 2.3: *Selection Criteria for the Luminous Galaxy (LG) Sample*[a]

Sample	Selection	EW Hα	Sérsic n	colour-cut	N_{gal}
LG1	Hα	< 0	...	...	30,744
LG2	Sérsic	...	> 2	...	68,482
LG3	Sérsic + colour-cut	...	> 2	$3\sigma_{\rm MAD}$ of CMR	52,447

[a] The Luminous Galaxy (LG) sample includes 82,171 objects. The sample LG1, LG2 & LG3 implement the same selection criteria as the MG samples listed in Table 2.2 with an additional cut in absolute magnitude ($M_{r'} < -21.0$) used over the entire redshift range of $0.05 < z \leq 0.15$.

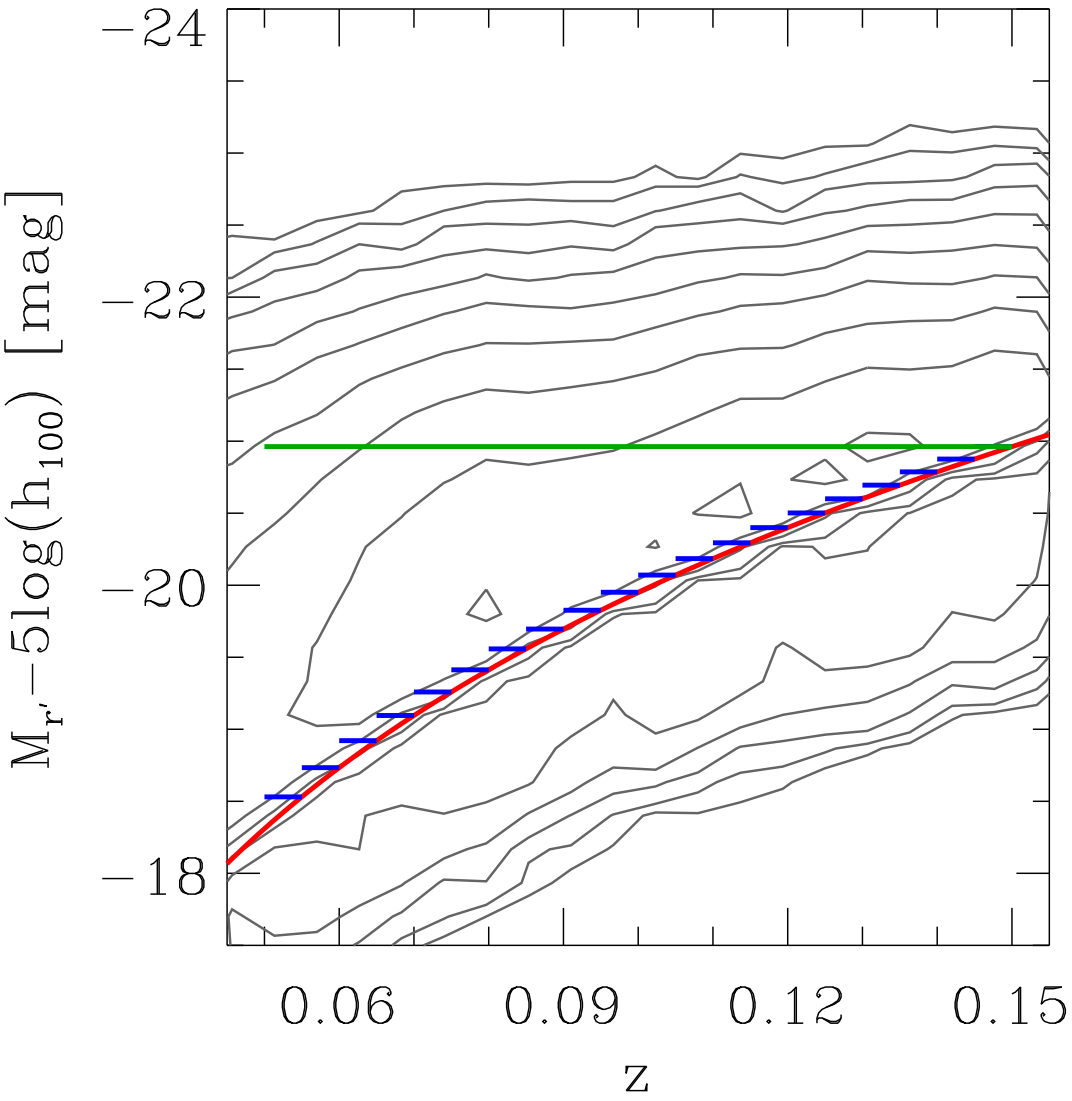

Figure 2.1: The absolute Petrosian magnitude distribution of all NYU Catalog galaxies from the DR6 in redshift space (contours). The red solid curve is the completeness limit of the SDSS instrument in the r'-band. The redshift dependent cuts in absolute magnitude $M_{r'}$ in each redshift bin of the Main Galaxy (MG) sample are represented by the blue solid lines of width $\triangle z = 0.005$. The green solid line of $\triangle z = 0.1$ is the $M_{r'}$-cut of the Luminous Galaxy (LG) sample (see Tables 2.1 & 2.3). The median redshift of the SDSS main galaxy sample is ~ 0.1.

Chapter 3

Results

We now want to compare and analyse our 3 galaxy samples in different parameter spaces. The Tables 3.1 - 3.7 present the results of MG1, MG2 & MG3 over the entire redshift range of $0.05 < z \leq 0.15$. The shown diagrams in Figures 3.1 - 3.5 reflect only the data of the $0.060 < z \leq 0.065$ redshift bin. We chose to present the figures of this particular redshift bin because it includes a high number of galaxies and covers a magnitude range of at least 3.5 magnitudes (see Table 2.1). At $z < 0.06$ the MG sample contains fewer objects, and if $z > 0.07$ the covered magnitude range decreases below 3.5 magnitudes.

3.1 Main Galaxy Samples: Colour-magnitude relation

Analysing each sample's concentration in CM-space enable us to judge which criterion selects the tightest and most reliable sample of red sequence galaxies. This can also be seen as a first step in our evaluation of the selection criteria as age separators; stellar old early-type objects form a tight red sequence (Degiola-Eastwood 1980 [16], Merluzzi *et al.* 2002 [39], Weinmann *et al.* 2006 [52]). An extended red sequence on the other hand suggests that we include star forming & stellar younger systems in our sample.

We use apparent colours & magnitudes in this section to minimise bias effects in our analysis. Biases could be introduced by making assumptions on model parameters like Ω_0, Ω_Λ, or H_0 which are needed to calculate absolute values.

The MG1 sample shows a tight red sequence (top panel of Figure 3.1) with a fitted colour-magnitude relation (CMR) of slope m = -0.019 (red solid line) and a low scatter of $\sigma_{\mathrm{MAD}} \sim 0.05$ around this CMR. The CMR of MG1 is calculated with an iterative σ_{MAD}-clipping linear least squares fit, a robust fitting method which is also used to calculate the CMRs of all other samples. As we can see in Table 3.1 the CMR slope of MG1 stays nearly constant with z, varying only slightly around $m \sim 0.02$ between the different redshift bins. The slope's 1σ error is of the same magnitude as the slope value itself, increasing little from 0.02 to 0.05 with

redshift z. This error increases with z due to the loss of brightness coverage caused by the higher luminosity limits $M_{r'}$ (blue lines in Figure 2.1) and the redshift effect on the galaxy colour (K-correction, see Hogg *et al.* 2002 [30]). The MG1 sample is spread over a larger colour but less magnitude range at higher z making the sample's CM-space concentrationthe more clumpy and the CMR-fit less reliable (increase of calculated error). This results also in a z dependent increase of the σ_{MAD} scatter parameter. The error of the σ_{MAD} value is low and independent of z. It is estimated by us using the Jack-Knife resampling method (e.g. see Miller 1974 [40]).
The increase of the CMR's normalisation n is due to the redshift effect on the galaxy colour $(g' - r')$. Early-type galaxies appear redder in colour at higher z because their continuum SED is redshifted inside the instrument's rest frame filter band system resulting in a z dependent reddening of the galaxy colour (K-correction).
Note, that the here discussed reasons for the z dependent increases of σ of m, n and σ_{MAD} are also valid for the other two samples of MG2 & MG3.
Independent of redshift effects or the limits on magnitude coverage, the MG1 sample shows a tight red sequence with a strong CMR, therefore it is reasonable to use its $3\sigma_{\mathrm{MAD}}$-limit as a colour-cut in our later effort to exclude blue early-type galaxies from the morphology selected sample (MG2).
The red sequence of the MG2 sample is plotted in the mid panel of Figure 3.1, and its data is listed in Table 3.2. The CMR of MG2 (solid green line) has a slope m of -0.021. For comparison, we plot the CMR of MG1 in this panel as well (red solid line with $m =$ -0.019). MG1 & MG2 feature nearly identical CMRs, only a little offset of about 0.02 in normalisation n separates them. The MG2 red sequence shows a high scatter ($\sigma_{\mathrm{MAD}} = 0.1$), twice the value of MG1 ($\sigma_{\mathrm{MAD}} \sim 0.05$). The high scatter is caused by the inclusion of many blue early-type galaxies, about 25% of the MG2 galaxies lie below the colour-cut (dotted red line in Figure 3.1) This colour-cut is the $3\sigma_{\mathrm{MAD}}$-limit of MG1 sample. Note, that only about 3% of the MG1 galaxies are located below this colour-cut.
The correctness of this colour-cut is backed by the histogram of Figure 3.2. It shows the colour residuals $\triangle(g' - r')$ of MG1 & MG2. The black solid line indicates the position of each sample's CMR. MG1 shows a symmetric and tight distribution around its CMR (criss-cross shaded distribution). Only 3% of the MG1 galaxies lie at the blue side of the colour-cut ($\triangle(g'-r') <$ -$3\sigma_{\mathrm{MAD}}$). In case of MG2 (open distribution) the majority of galaxies (75%) lie above the colour-cut, the rest of the sample galaxies form a tail of blue objects. The asymmetric distribution of MG2 in colour space $\triangle(g' - r')$ makes it impossible to use the ordinary Gaussian σ as scatter indicator. Only the robust σ_{MAD} quantity is capable to represent the sample's scatter properly. That is the reason why we use the σ_{MAD}-value as scatter parameter throughout all galaxy samples, making the comparison between the samples reliable and concise.
The red sequence of MG3 is shown in the lower panel of Figure 3.1, and its data can be

found in Table 3.3. The CMR of MG3 (blue solid line) is identical with the CMR of MG2 (in slope m & normalisation n). The MG3 CMR is also comparable with the CMR of MG1 showing only a small offset of ~ 0.02 in n. The scatter of the MG3 red sequence is with ~ 0.06 a bit higher than the scatter of MG1 ($\sigma_{\rm MAD} = 0.05$), but significantly less than the scatter of MG2 ($\sigma_{\rm MAD} \sim 0.1$).
The 3 CMRs of MG1, MG2 & MG3 are all consistent with each other, and all 3 are also in good agreement with the CMR slope of m = -0.022 found in the Sérsic $n > 2$ galaxy sample of [31]. The main differences between our three galaxy samples are the scatter of the different red sequences indicated by the $\sigma_{\rm MAD}$ value and the number of included galaxies. The galaxy number of MG1 is less than half the value of MG2 and $\sim 2/3$ the value of MG3. MG1 is the best selection of red sequence galaxies, given that it shows the lowest red sequence scatter even without introducing any "artificial" colour limit (exclusion of bluer galaxies). It is also the sample with the lowest galaxy number, suggesting that the Hα-absorption criterion selects only the "core" galaxies of the red sequence.

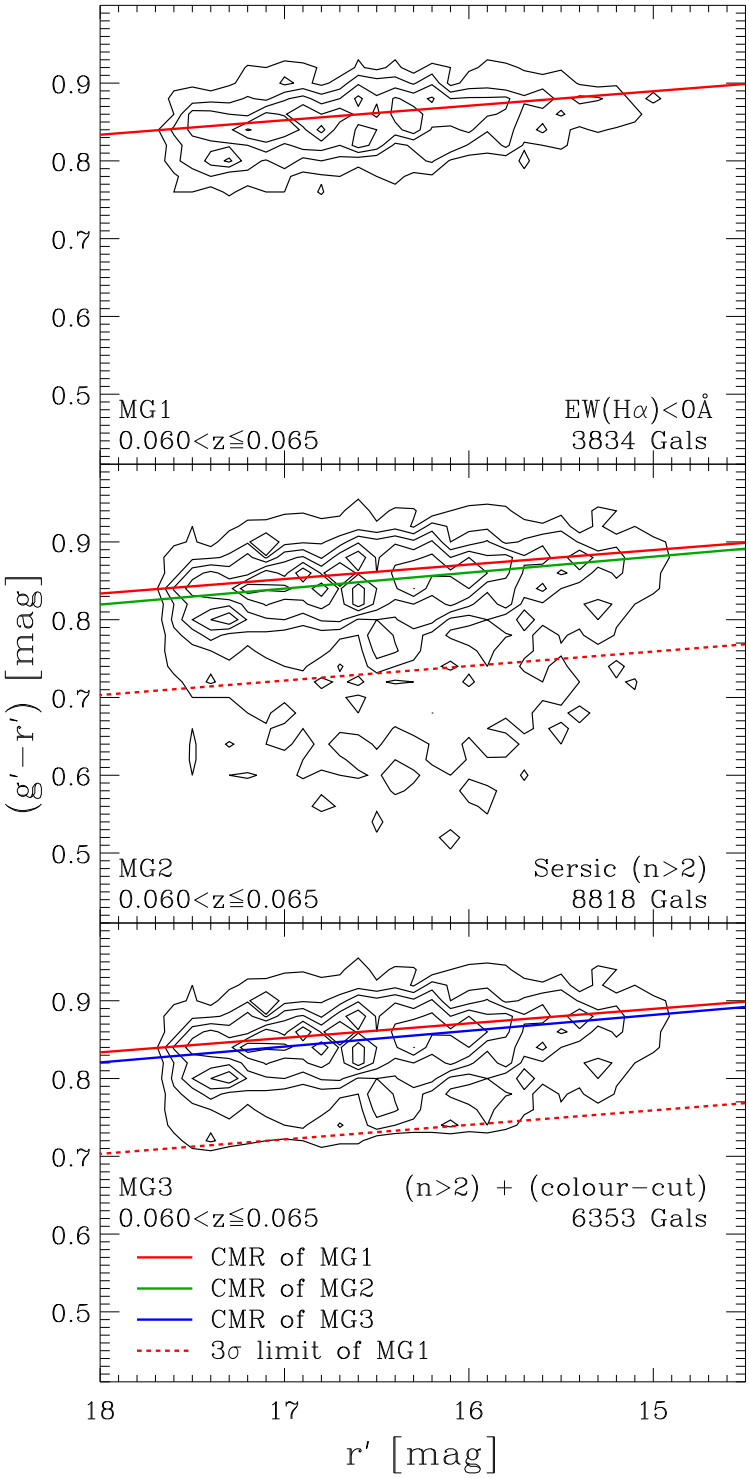

Figure 3.1: The colour-magnitude (CM) diagrams of MG1, MG2, and MG3 at $0.060 < z \leq 0.065$. All solid drawn lines are sigma-clipped least squares fit to the plotted galaxy populations. The red solid line is MG1's fitted CM relation (upper panel), the green line the fitted CM relation of MG2 (middle panel), and the blue line is the CMR of MG3 (bottom panel). The dashed red line is the $3\sigma_{\mathrm{MAD}}$ limit of the colour residuals distribution $\triangle(g' - r')$ of MG1 with respect to its CMR (red solid line). The number of galaxies in each subsample is indicated in the different panels.

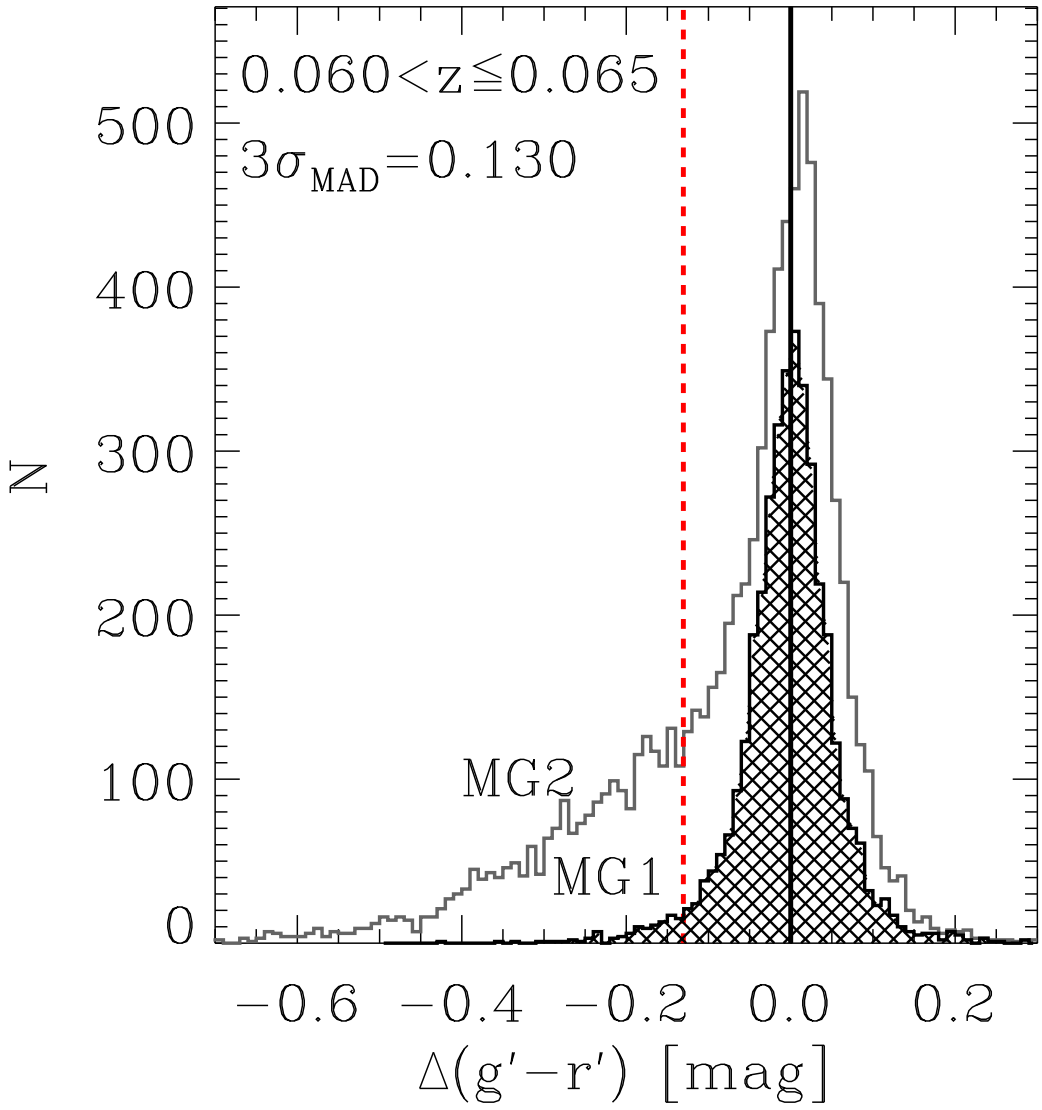

Figure 3.2: Colour residuals $\triangle(g'-r')$ of MG1 (hatched distribution) and MG2 (open) in the redshift range $0.060 < z \leq 0.065$ (see Figure 3.1). The red dotted line is the $3\sigma_{\rm MAD}$ limit of the MG1 colour residuals $\triangle(g'-r')$; it can be used as a selection criterion to exclude bluer galaxies from MG2 (the Sérsic sample). Note that the $3\sigma_{\rm MAD} \simeq 2\sigma$ of a Gaussian distribution and that we are only cutting at one side, therefore more than 97% of the MG1 galaxies (Hα EW<0Å) are redder than the colour-cut of $3\sigma_{\rm MAD}$.

Table 3.1: *Colour-magnitude relation: MG1*

$\triangle$z	f(N_{gal})[a]	$m \pm\sigma_m$[b]	$n \pm\sigma_n$[b]	$\sigma_{\rm MAD}[\triangle(g'-r')]$[c]
$0.050 < z \leq 0.055$	22.4% (2,985)	-0.020 ±0.024	1.17 ± 0.02	0.044 ±0.003
$0.055 < z \leq 0.060$	23.5% (2,914)	-0.018 ±0.026	1.15 ± 0.02	0.044 ±0.001
$0.060 < z \leq 0.065$	23.8% (3,834)	-0.019 ±0.024	1.17 ± 0.02	0.044 ±0.000
$0.065 < z \leq 0.070$	25.3% (4,146)	-0.018 ±0.023	1.17 ± 0.02	0.044 ±0.002
$0.070 < z \leq 0.075$	27.5% (5,222)	-0.017 ±0.022	1.17 ± 0.02	0.044 ±0.001
$0.075 < z \leq 0.080$	28.0% (5,487)	-0.015 ±0.022	1.15 ± 0.02	0.044 ±0.000
$0.080 < z \leq 0.085$	29.5% (5,855)	-0.017 ±0.023	1.20 ± 0.02	0.045 ±0.001
$0.085 < z \leq 0.090$	29.5% (4,993)	-0.014 ±0.025	1.16 ± 0.01	0.047 ±0.001
$0.090 < z \leq 0.095$	30.0% (4,338)	-0.015 ±0.028	1.19 ± 0.02	0.048 ±0.002
$0.095 < z \leq 0.100$	30.0% (4,280)	-0.014 ±0.030	1.20 ± 0.02	0.049 ±0.001
$0.100 < z \leq 0.105$	27.8% (3,751)	-0.015 ±0.032	1.21 ± 0.02	0.050 ±0.001
$0.105 < z \leq 0.110$	30.0% (4,010)	-0.017 ±0.032	1.27 ± 0.02	0.050 ±0.000
$0.110 < z \leq 0.115$	31.5% (4,509)	-0.018 ±0.032	1.29 ± 0.02	0.049 ±0.001
$0.115 < z \leq 0.120$	28.8% (3,839)	-0.014 ±0.035	1.24 ± 0.02	0.054 ±0.001
$0.120 < z \leq 0.125$	28.7% (3,357)	-0.019 ±0.040	1.34 ± 0.02	0.053 ±0.003
$0.125 < z \leq 0.130$	31.6% (3,775)	-0.016 ±0.039	1.30 ± 0.02	0.055 ±0.000
$0.130 < z \leq 0.135$	34.5% (4,178)	-0.014 ±0.038	1.29 ± 0.02	0.056 ±0.001
$0.135 < z \leq 0.140$	36.3% (3,936)	-0.021 ±0.039	1.42 ± 0.02	0.055 ±0.001
$0.140 < z \leq 0.145$	36.8% (3,447)	-0.019 ±0.044	1.41 ± 0.02	0.055 ±0.003
$0.145 < z \leq 0.150$	36.7% (3,205)	-0.023 ±0.047	1.49 ± 0.02	0.056 ±0.002

[a] The fraction of EW H$\alpha < 0$Å galaxies inside each redshift bin. The value in parentheses is the selected number of galaxies (see Table 2.1).

[b] The slope (m) and normalization (n) of the linear colour-magnitude relation $(g - r) = n + mr$ and its 1σ errors.

[c] The $1\sigma_{\rm MAD}$ of the colour residual's distribution $\triangle(g' - r')$ and its error. The error was calculated using the Jack-knife resampling method (Miller 1974 [40]).

Table 3.2: *Colour-magnitude relation: MG2*

$\triangle$z	f(N_{gal})[a]	$m \pm\sigma_m$[b]	$n \pm\sigma_n$[b]	$\sigma_{\rm MAD}[\triangle(g'-r')]$[c]
$0.050 < z \leq 0.055$	50.9% (6,768)	-0.019 ±0.019	1.14 ± 0.01	0.102 ±0.008
$0.055 < z \leq 0.060$	52.2% (6,489)	-0.018 ±0.020	1.14 ± 0.02	0.098 ±0.002
$0.060 < z \leq 0.065$	54.7% (8,818)	-0.021 ±0.018	1.19 ± 0.01	0.096 ±0.001
$0.065 < z \leq 0.070$	55.7% (9,115)	-0.020 ±0.018	1.19 ± 0.01	0.095 ±0.002
$0.070 < z \leq 0.075$	58.9% (11,188)	-0.017 ±0.017	1.16 ± 0.01	0.090 ±0.002
$0.075 < z \leq 0.080$	60.5% (11,870)	-0.016 ±0.017	1.16 ± 0.01	0.090 ±0.002
$0.080 < z \leq 0.085$	63.0% (12,518)	-0.018 ±0.018	1.21 ± 0.01	0.093 ±0.001
$0.085 < z \leq 0.090$	63.8% (10,778)	-0.016 ±0.020	1.18 ± 0.01	0.094 ±0.000
$0.090 < z \leq 0.095$	63.9% (9,220)	-0.016 ±0.023	1.19 ± 0.01	0.099 ±0.001
$0.095 < z \leq 0.100$	65.8% (9,378)	-0.017 ±0.024	1.23 ± 0.01	0.098 ±0.001
$0.100 < z \leq 0.105$	65.9% (8,875)	-0.021 ±0.025	1.30 ± 0.01	0.102 ±0.002
$0.105 < z \leq 0.110$	67.3% (8,989)	-0.022 ±0.025	1.33 ± 0.01	0.101 ±0.004
$0.110 < z \leq 0.115$	70.0% (10,035)	-0.024 ±0.025	1.37 ± 0.01	0.104 ±0.002
$0.115 < z \leq 0.120$	70.5% (9,395)	-0.019 ±0.027	1.31 ± 0.01	0.110 ±0.002
$0.120 < z \leq 0.125$	70.3% (8,218)	-0.025 ±0.030	1.42 ± 0.01	0.114 ±0.003
$0.125 < z \leq 0.130$	72.5% (8,653)	-0.026 ±0.030	1.46 ± 0.01	0.114 ±0.004
$0.130 < z \leq 0.135$	75.3% (9,130)	-0.029 ±0.030	1.52 ± 0.01	0.114 ±0.002
$0.135 < z \leq 0.140$	76.9% (8,343)	-0.034 ±0.033	1.63 ± 0.01	0.113 ±0.002
$0.140 < z \leq 0.145$	77.4% (7,249)	-0.031 ±0.036	1.59 ± 0.02	0.113 ±0.003
$0.145 < z \leq 0.150$	78.6% (6,865)	-0.040 ±0.039	1.77 ± 0.02	0.115 ±0.000

[a] The fraction of Sérsic $n > 2$ galaxies inside each redshift bin. The value in parentheses is the selected number of galaxies (see Table 2.1).

[b] The slope (m) and normalization (n) of the linear colour-magnitude relation $(g-r) = n + mr$ and its 1σ errors.

[c] The $1\sigma_{\rm MAD}$ of the colour residual's distribution $\triangle(g'-r')$ and its error. The error was calculated using the Jack-knife resampling method (Miller 1974 [40]).

Table 3.3: *Colour-magnitude relation: MG3*

$\triangle$z	f(N_{gal})[a]	$m \pm\sigma_m$[b]	$n \pm\sigma_n$[b]	$\sigma_{\rm MAD}[\triangle(g'-r')]$[c]
$0.050 < z \leq 0.055$	35.7% (4,752)	-0.019 ±0.019	1.15 ± 0.01	0.054 ±0.000
$0.055 < z \leq 0.060$	37.2% (4,620)	-0.018 ±0.020	1.14 ± 0.02	0.055 ±0.001
$0.060 < z \leq 0.065$	39.4% (6,353)	-0.020 ±0.018	1.19 ± 0.01	0.054 ±0.003
$0.065 < z \leq 0.070$	40.2% (6,580)	-0.020 ±0.018	1.19 ± 0.01	0.054 ±0.002
$0.070 < z \leq 0.075$	43.8% (8,317)	-0.017 ±0.017	1.16 ± 0.01	0.053 ±0.001
$0.075 < z \leq 0.080$	44.7% (8,766)	-0.016 ±0.017	1.15 ± 0.01	0.053 ±0.001
$0.080 < z \leq 0.085$	47.1% (9,360)	-0.019 ±0.018	1.22 ± 0.01	0.056 ±0.000
$0.085 < z \leq 0.090$	48.2% (8,138)	-0.016 ±0.020	1.18 ± 0.01	0.058 ±0.002
$0.090 < z \leq 0.095$	47.5% (6,863)	-0.016 ±0.023	1.20 ± 0.01	0.059 ±0.000
$0.095 < z \leq 0.100$	49.4% (7,047)	-0.016 ±0.024	1.22 ± 0.01	0.060 ±0.001
$0.100 < z \leq 0.105$	49.2% (6,625)	-0.020 ±0.025	1.29 ± 0.01	0.062 ±0.001
$0.105 < z \leq 0.110$	50.5% (6,745)	-0.021 ±0.025	1.32 ± 0.01	0.063 ±0.004
$0.110 < z \leq 0.115$	51.3% (7,360)	-0.021 ±0.025	1.34 ± 0.01	0.061 ±0.000
$0.115 < z \leq 0.120$	52.9% (7,045)	-0.019 ±0.027	1.31 ± 0.01	0.068 ±0.001
$0.120 < z \leq 0.125$	51.6% (6,031)	-0.024 ±0.031	1.41 ± 0.01	0.068 ±0.002
$0.125 < z \leq 0.130$	53.7% (6,408)	-0.024 ±0.031	1.43 ± 0.01	0.068 ±0.001
$0.130 < z \leq 0.135$	56.7% (6,875)	-0.026 ±0.030	1.47 ± 0.01	0.071 ±0.001
$0.135 < z \leq 0.140$	57.3% (6,222)	-0.031 ±0.033	1.59 ± 0.01	0.068 ±0.001
$0.140 < z \leq 0.145$	57.7% (5,402)	-0.029 ±0.036	1.56 ± 0.02	0.069 ±0.001
$0.145 < z \leq 0.150$	58.3% (5,092)	-0.038 ±0.039	1.73 ± 0.02	0.069 ±0.002

[a] The fraction of galaxies that have Sérsic $n > 2$ and colour deviation $\triangle(g'-r') > -3\sigma_{\rm MAD}$ in each redshift bin (see Figure 3.1, middle and bottom panels). The value in parentheses is the selected number of galaxies (see Table 2.2).

[b] The slope (m) and normalization (n) of the linear colour-magnitude relation $(g-r) = n + mr$ and its 1σ errors.

[c] The $1\sigma_{\rm MAD}$ of the colour residual's distribution $\triangle(g'-r')$ and its error. The error was calculated using the Jack-knife resampling method (Miller 1974 [40]).

3.2 Main Galaxy Samples: Fractions

To clarify how restrictive our applied selection criteria are, we look into the galaxy amount of every sample. The sample sizes are given by $f(N_{gal})$, that is the fraction of each sample's galaxy number with respect to the total galaxy number of the Main Galaxy (MG) sample (see Tables 2.1 & 3.1 - 3.3).
The sample fractions depend on the applied selection criteria. The Hα-selection (MG1) includes up to 37% of the galaxies (Table 3.1), the MG2 sample up to 79% (Table 3.2), and MG3 selection up to 59% (Table 3.3). These 3 here presented sample fractions of $f(N_{gal})$ are upper limits. They are redshift dependent and increase with z due to the changing luminosity limits of $M_{r'}$ (see Figure 2.1); at higher z only more luminous galaxies are detectable. It is known that the most luminous (and also massive) objects are more likely to be non-star forming systems (Feulner *et al.* 2005 [22], Feulner *et al.* 2006 [23]), therefore the fraction of non-star forming objects inside our 3 samples increases with z. Note that the apllied selection criteria are designed to identify early-type non-starforming red sequence objects, therefore they will cover a higher fraction of galaxies ($f(N_{gal})$) at higher redshifts.
Looking into all 20 redshift bins, MG1 includes the fewest galaxies showing the lowest fraction of included galaxies. Nearly all objects included in MG1 can also be found inside MG2 & MG3; $\sim$ 99% of the MG1 galaxies are included in MG2 and about 96% of the MG1 sample is included in MG3. MG2 & MG3 are also including Hα-active galaxies, therefore the fraction of Hα-passive galaxies lie for these two samples only at 45% (MG2) & 60% (MG3).
The MG3 sample includes only 75% of the MG2 galaxies. About 25% of the MG2 galaxies have bluer colours and are excluded by the additional applied colour-cut. However, MG3 consists of significant more galaxies than MG1.
As we can see the Hα-criterion is the most restrictive one. The Hα-sample (MG1) is the smallest sample in terms of galaxy number (N_{gal}) featuring only passive, non-starforming objects. The selection criteria of Sérsic n and colour (MG2 & MG3) select nearly all Hα-absorbers of MG1 as well, but they are also selecting possible starforming objects (EW(Hα) > 0Å).

3.3 MG Samples: Spectral properties

Every galaxy plotted in Figure 3.1 has a measured spectrum. These are used to construct the luminosity weighted average spectra presented in Figure 3.3. Using these average spectra allow us to examine if and how our 3 galaxy samples are contaminated by star forming and stellar younger objects. Note, that for galaxies with $z \geq 0.6$ the O[II]-line at 3750Å is located inside the observed optical spectrum of SDSS (reliable line measurement). This O[II] spectral line is an additional well established indicator of the galaxy's current star formation.

We measure the 4000Å-break (D4000-flux ratio) of every average spectra to estimate later in Section 3.5 the average stellar age of every galaxy sample. This will then help us to clarify which selection criteria is the best age indicator.

The average spectrum of MG1 is shown in the upper panel of Figure 3.3. It features the absorption lines of Hα, Hβ, N[II], O[II] & [OIII] and shows no significant emission line in the 3700Å - 6800Å optical rest-frame spectrum. The 4000Å-break is, judged by its D4000-flux ratio of 1.73, highly elevated and the SED's continuum shape is that of an early-type galaxy (increasing flux towards higher wavelengths).

The MG1 average spectrum is a prime example of a passively aged galaxy. Its high 4000Å-break and the absorption line features suggest that the MG1 consists mainly of galaxies with stellar old populations. Based on the Hα and O[II]-absorption lines there is no indication of any ongoing star formation activity inside this sample.

The mid panel of Figure 3.3 presents the average spectrum of MG2. It shows strong emissions in Hα and O[II]. Less active emission lines visible inside this spectrum are the [OIII], [NII] and Hβ line. The SED continuum shape is flattened and shows with a D4000-value of 1.54 a less elevated 4000Å-break than in MG1. All these spectral characteristics suggest that we have included a notable fraction of starforming and stellar younger galaxies in this sample.

The average spectrum of MG3 can be found in the lower panel of Figure 3.3. Its SED continuum shape and its D4000-value of 1.68 (4000Å-break) are comparable with the values found in MG1. Additionally, the indicated Hβ-absorption line of MG3 looks alike the Hβ-absorption line of MG1. The differences between the average spectra of MG1 & MG3 are visible if one looks at the Hα, O[II] and N[II] spectral lines; all 3 lines are passive in the MG1 spectrum but show a uniform sized emission in the spectrum of MG3. These equal and simultaneous line emissions inside the MG3 spectrum suggest that the sample's net line emission is dominated by AGN galaxies (see Section 3.4). The O[III]-line of MG3 shows only small emission activity. This quantity is different in all 3 samples; MG1 has O[III] in absorption, MG2 shows strong line emission in O[III], and MG3 features only half the O[III]-line emission of MG2.

Comparing the spectra of MG2 & MG3 with each other suggests that the applied colour-cut (described in Section 3.1) is a handy tool to exclude starforming and stellar young early-type galaxies from a Sérsic (morphology) selection. The 4000Å-break of MG3 is higher than the one of MG2, and the emissions in Hα, O[II] and [OIII] are also less developed in the spectrum of MG3 than in MG2. The SED continuum shape of MG3 shows clearly early-type character, the MG2 SED continuum shape on the other hand is flattened and untypical for an early-type galaxy.

Comparing all sample spectra with each other allows one conclusion: selecting by colour & Sérsic n is not as effective in the identification of passive objects than using the single spectral criterion of Hα absorption. The MG1 spectrum features the highest 4000Å-break,

the deepest Hα, Hβ & O[III] absorption lines and the lowest emission activity of all samples. The 4 spectral lines indicated in Figure 3.3 allow us to calculate each sample's fraction of star forming and AGN galaxies (Section 3.4) by using BPT diagnostics (Baldwin *et al.* 1981 [2]). This method demands that all 4 spectral lines (Hα, Hβ, [NII], [OIII]) are simultaneously in emission. For this reason we cannot apply the BPT diagnostic on MG1; all MG1 galaxies are by definition Hα-absorbers, therefore we have no detectable sign of star formation or AGN activity inside this sample.

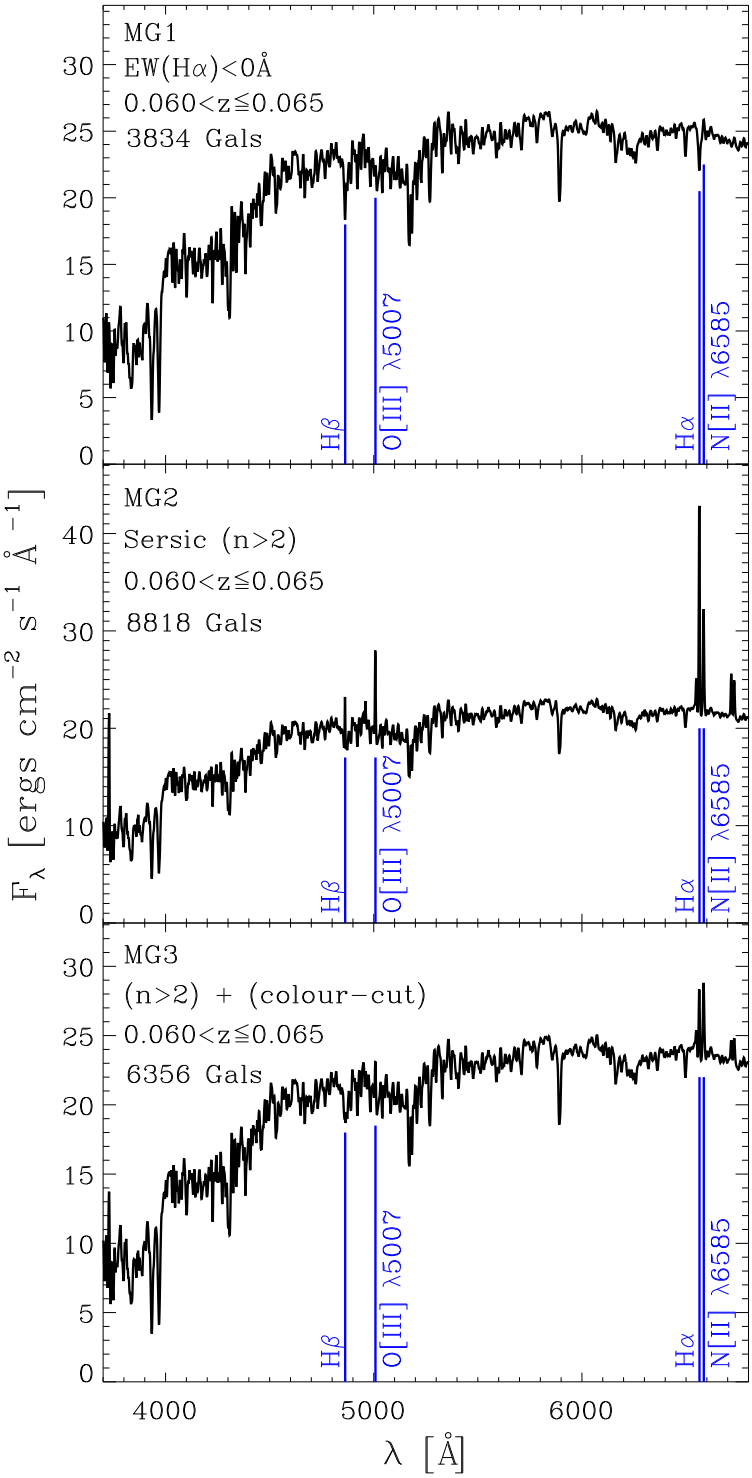

Figure 3.3: Luminosity weighted stacked spectra of MG1 (top panel), MG2 (middle panel) and MG3 (bottom panel) at rest-frame wavelength λ in the redshift range $0.060 < z \leq< 0.065$. The spectral lines used in the diagnostic of the BPT-diagrams are indicated here with blue lines. The average spectrum of MG1 shows no emission in any of these 4 lines. In contrast, the other two samples show measurable line emission, except for the Hβ absorption feature in the case of MG3. The spectra's continuum shapes and absorption features indicate that the Hα-selection (MG1) identifies on average the oldest galaxy population.

3.4 MG Samples: AGN vs. Star formation

We do not know exactly how AGNs effect the stellar population of galaxies, if their feedback is preventing or supporting star formation in galaxies. Sometimes it is also unclear if a galaxy's emission in Hα or [OII] is caused by an AGN or star formation activity. However, it is of importance to know how many AGN and/or star forming galaxies are included in a galaxy selection. Remember, we are not only looking for the stellar oldest objects of the local Universe, but also for a galaxy sample most uniform in age. In this manner, any sample contamination by star forming galaxies should be avoided or eliminated.
The galaxies of MG1 are by definition all Hα-absorbers, therefore we do not have any star formation in this selection. Due to the sample's Hα-inactivity it is not possible to calculate the AGN fraction of this sample by using BPT-diagnostics (see Baldwin *et al.* 1981 [2]). This method requires that Hα, Hβ, [NII], and [OIII] are simultaneously in emission which is not the case in MG1 (see Section 3.3).
MG2 & MG3 possess galaxies with simultaneous emission in all these 4 lines (active galaxies). The sample fraction of active galaxies f(N_{active}) can rise up to 32% for MG2 (Table 3.4) and 13% for MG3 (Table 3.5). These fraction values, calculated with respect to the total galaxy number N_{gal} of each sample (see Tables 3.2 & 3.3), are upper limits and decrease with z due to the higher luminosity limits $M_{r'}$ at higher redshifts (see Figure 2.1). The higher luminosity limits at higher z disadvantage the inclusion of starforming galaxies, therefore the sample fraction of MG2 & MG3 of active galaxiex f(N_{active}) decreases with z.
Figure 3.4 presents the BPT-diagrams of MG2 (left panel) and MG3 (right panel). We classify active galaxies into 3 categories using the separation curves of Kauffmann *et al.* 2003 [34] (black solid line) and Kewley *et al.* 2001 [38] (grey dashed line). Our 3 classes are starforming galaxies (SF), AGN dominated galaxies (AGN) and hybrid galaxies (AGN/SF). For the latter mentioned class the line ratios of [NII]/Hα and [OIII]/Hβ cannot help us to distinguish clearly enough between pure star formation and AGN activity, therefore, their emission character can only be described as hybridly. The blue squares in Figure 3.4 represent starforming galaxies (SF), the red diamonds are AGN dominated galaxies (AGN), and the green triangles represent the hybrid galaxies (AGN/SF). The sample fraction of these 3 galaxy classes are calculated with respect to each sample's total galaxy number N_{gal} (see Tables 3.2 & 3.3) and are shown in lower left corner of each panel. These sample fractions of MG2 & MG3 and their dependence on redshift can be found in Tables 3.4 & 3.5.
In Table 3.4 one can see how the luminosity limits of $M_{r'}$ affect the selection of starforming early-type galaxies (MG2 sample). The MG2 fraction of SF galaxies drops from 15% to 2% while going from $M_{r'} <$ -18.5 to $M_{r'} <$ -21.0 in the redshift range of $0.05 < z \leq 0.15$. The sample's AGN fraction on the other hand is only changing from 6% to 4%, and the sample's fraction of AGN/SF galaxies cuts nearly in half going from 11.2% to 6.2%. This significant change can be explained again by the luminosity based loss of mainly starforming galaxies in

our sample ($M_{r'}$ luminosity cuts). We conclude therefore, that AGN galaxies are on average brighter than their starforming counterparts and are for that reason also less effected by changing $M_{r'}$-cuts/luminosity limits. Therefore, higher luminousity limits will not effectivly exclude AGN dominated galaxies from a Sérsic selected sample of early-type galaxies.
The colour-cut of MG3 is capable of excluding SF and AGN/SF galaxies from an early-type galaxy sample (see Table 3.5). The fractions of star forming and AGN/SF galaxies in MG3 is significantly lower than in MG2; in MG2 the maximal fractions are 15% (SF) & 11% (AGN/SF), in MG3 the maximal fractions are only 2% (SF) & 6% (AGN/SF). The AGN fraction of both samples are with maximal 6% (MG2) & 5% (MG3) close to each other. Based on these numbers, one can conclude that early-type AGNs are primarily settled inside the red sequence and early-type SF and AGN/SF galaxies are primarily located at the "blue" edge of the red sequence.
In Table 3.5 one can also see, that pure starforming galaxies (SF) are only a minority in MG3 and that AGN and AGN/SF objects are the dominant fraction among MG3's active galaxies. At higher redshifts ($z > 0.1$) the AGN fraction of MG3 even outruns the sample's fraction of hybrid AGN/SF galaxies. The AGN domination among the active MG3 galaxies is even visible in the sample's average spectrum (lower panel of Figure 3.3); equal emission in Hα and [NII].
Knowing now the contamination by star forming and AGN galaxies inside the MG2 & MG3 sample, we can see now that the Hα-selected sample is the most purest galaxy selection of non-star forming galaxies. Even eliminating all AGN, SF and AGN/SF objects from the MG2 & MG3 samples will not reduce the sample's total galaxy number too such low values comparable to MG1. The MG1 sample will remain the red sequence sample with the lowest galaxy number. That leads to the idea that MG2 & MG3 include also a notable number of Hα-emitting galaxies (at least EW(Hα) > 0Å) which have simultaneously at least one of the 3 lines of Hβ, N[II] or O[III] in absorption. These galaxies are possible transition objects which arrived on the red sequence recently due to their recently ended star formation but did not yet achieved full Hα-passiveness until now.

Table 3.4: *AGN fraction: MG2*[a]

$\triangle$z	f($N_{\rm active}$)[b]	f($N_{\rm AGN}$)[c]	f($N_{\rm AGN/SF}$)[d]	f($N_{\rm SF}$)[e]
$0.050 < z \leq 0.055$	31.7% (2,144)	5.8% (392)	11.2% (755)	14.7% (997)
$0.055 < z \leq 0.060$	29.6% (1,920)	5.7% (369)	11.4% (739)	12.5% (812)
$0.060 < z \leq 0.065$	28.5% (2,509)	6.0% (526)	11.4% (1,001)	11.1% (982)
$0.065 < z \leq 0.070$	26.9% (2,450)	5.3% (482)	11.1% (1,016)	10.4% (952)
$0.070 < z \leq 0.075$	24.5% (2,736)	5.1% (570)	10.3% (1,150)	9.1% (1,016)
$0.075 < z \leq 0.080$	22.9% (2,720)	4.9% (582)	10.2% (1,210)	7.8% (928)
$0.080 < z \leq 0.085$	22.0% (2,752)	5.0% (628)	10.3% (1,293)	6.6% (831)
$0.085 < z \leq 0.090$	20.6% (2,224)	4.4% (477)	10.1% (1,089)	6.1% (658)
$0.090 < z \leq 0.095$	20.4% (1,882)	4.9% (450)	9.7% (898)	5.8% (534)
$0.095 < z \leq 0.100$	20.7% (1,939)	5.8% (540)	9.8% (916)	5.2% (483)
$0.100 < z \leq 0.105$	20.6% (1,829)	5.8% (511)	9.8% (867)	5.1% (451)
$0.105 < z \leq 0.110$	19.1% (1,715)	5.3% (475)	9.0% (810)	4.8% (430)
$0.110 < z \leq 0.115$	16.0% (1,605)	5.4% (542)	7.1% (715)	3.5% (348)
$0.115 < z \leq 0.120$	17.6% (1,650)	5.2% (485)	8.4% (791)	4.0% (374)
$0.120 < z \leq 0.125$	17.6% (1,450)	5.3% (434)	8.2% (671)	4.2% (345)
$0.125 < z \leq 0.130$	17.1% (1,481)	5.1% (442)	7.9% (681)	4.1% (358)
$0.130 < z \leq 0.135$	14.9% (1,362)	4.8% (439)	7.0% (636)	3.1% (287)
$0.135 < z \leq 0.140$	14.5% (1,209)	4.5% (375)	7.1% (595)	2.9% (239)
$0.140 < z \leq 0.145$	13.0% (942)	4.5% (326)	6.2% (446)	2.3% (170)
$0.145 < z \leq 0.150$	12.6% (864)	4.3% (293)	6.2% (427)	2.1% (144)

[a] MG2 only consists of galaxies that have Sérsic n > 2 in the r-band. The fractions are relative to the total number of MG2 galaxies in the same redshift bin.
[b] The fraction of galaxies inside each redshift bin of the MG sample which have emission in Hα, Hβ, N[II], and O[III] with a S/N > 2. The value in parentheses is the selected number of galaxies.
[c] The fraction of pure AGN dominated galaxies identified by the separation line of Kewley *et al.* 2001 [38] (see Fig. 3.4). The value in parentheses is the selected number of galaxies.
[d] The fraction of mixed AGN/starforming galaxies identified by the separation lines of Kauffmann *et al.* 2003 [34] and Kewley *et al.* 2001 [38] (see Fig. 3.4) The value in parentheses is the selected number of galaxies.
[e] The fraction of star-forming galaxies identified by the separation line of Kauffmann *et al.* 2003 [34] (see Fig. 3.4). The value in parentheses is the selected number of galaxies.

Table 3.5: *AGN fraction: MG3*[a]

$\triangle$z	f(N_{active})[b]	f(N_{AGN})[c]	f($N_{\mathrm{AGN/SF}}$)[d]	f(N_{SF})[e]
$0.050 < z \leq 0.055$	13.0% (618)	4.7% (224)	6.0% (287)	2.3% (107)
$0.055 < z \leq 0.060$	12.1% (560)	4.4% (203)	6.0% (277)	1.7% (80)
$0.060 < z \leq 0.065$	11.6% (735)	4.5% (286)	5.5% (351)	1.5% (98)
$0.065 < z \leq 0.070$	10.7% (704)	4.1% (270)	5.3% (347)	1.3% (87)
$0.070 < z \leq 0.075$	9.3% (772)	3.4% (285)	4.7% (389)	1.2% (98)
$0.075 < z \leq 0.080$	8.4% (739)	3.3% (286)	4.4% (382)	0.8% (71)
$0.080 < z \leq 0.085$	8.2% (768)	3.0% (284)	4.4% (416)	0.7% (68)
$0.085 < z \leq 0.090$	7.6% (620)	2.8% (226)	4.2% (340)	0.7% (54)
$0.090 < z \leq 0.095$	7.6% (521)	3.1% (212)	3.8% (262)	0.7% (47)
$0.095 < z \leq 0.100$	7.3% (511)	3.5% (245)	3.2% (225)	0.6% (41)
$0.100 < z \leq 0.105$	7.3% (481)	3.6% (238)	3.1% (206)	0.6% (37)
$0.105 < z \leq 0.110$	6.5% (436)	3.2% (218)	2.8% (186)	0.5% (32)
$0.110 < z \leq 0.115$	4.6% (340)	2.7% (200)	1.7% (123)	0.2% (17)
$0.115 < z \leq 0.120$	5.7% (400)	3.0% (212)	2.3% (162)	0.4% (26)
$0.120 < z \leq 0.125$	5.7% (346)	2.9% (176)	2.5% (149)	0.3% (21)
$0.125 < z \leq 0.130$	5.3% (340)	2.7% (174)	2.2% (141)	0.4% (25)
$0.130 < z \leq 0.135$	4.3% (298)	2.4% (166)	1.6% (111)	0.3% (21)
$0.135 < z \leq 0.140$	3.7% (233)	2.1% (129)	1.5% (96)	0.1% (8)
$0.140 < z \leq 0.145$	3.1% (169)	1.9% (102)	1.2% (63)	0.1% (4)
$0.145 < z \leq 0.150$	3.8% (194)	2.2% (112)	1.5% (75)	0.1% (7)

[a] MG3 only consists of galaxies that have Sérsic $n > 2$ in the r-band and colour deviation $\triangle(g' - r') > -3\sigma_{\mathrm{MAD}}$ (see Figure 3.1, middle and bottom panels). The fractions are calculated to the total number of MG3 galaxies in the same redshift bin.

[b] The fraction of galaxies inside each redshift bin which have emission in Hα, Hβ, N[II], and O[III] with a S/N > 2. The value in parentheses is the selected number of galaxies.

[c] The fraction of pure AGN dominated galaxies identified by the separation line of *et al.* 2001 [38] (see Fig. 3.4). The value in parentheses is the selected number of galaxies.

[d] The fraction of mixed AGN/starforming galaxies identified by the separation lines of Kauffmann *et al.* 2003 [34] and Kewley *et al.* 2001 [38] (see Fig. 3.4). The value in parentheses is the selected number of galaxies.

[e] The fraction of star-forming galaxies identified by the separation line of Kauffmann *et al.* 2003 [34] (see Fig. 3.4). The value in parentheses is the selected number of galaxies.

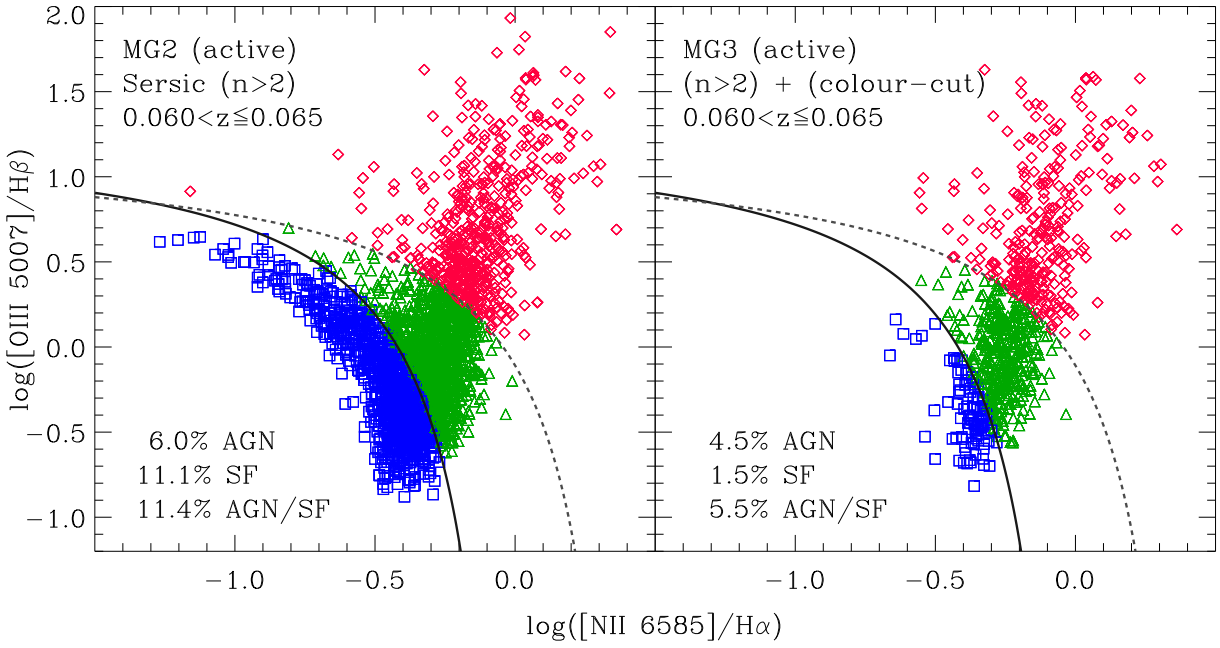

Figure 3.4: The BPT-diagrams of the active galaxies in MG2 (left panel) and MG3 (right panel) in the redshift range of $0.060 < z \leq 0.065$. The black solid line represents the separation curve of Kauffmann *et al.* 2003 [34] and the grey dashed-dotted one the separation curve of Kewley *et al.* 2001 [38]. "Pure" starforming galaxies (SF) are represented by blue squares, the green triangles are the hybrid AGN/SF galaxies, and the red diamonds count for AGN dominated galaxies (AGN). The 3 fractions shown in the lower left corner of each panel indicate the amount of active galaxies (AGN, SF & AGN/SF) inside each sample. These fractions are calculated with respect to the total galaxy number of each sample (MG2 & MG3). Applying the colour-cut (MG3) reduces the fraction of starforming and AGN/star-forming galaxies significantly, but there is still measurable contamination from active galaxies inside the sample.

3.5 MG Samples: D4000 distribution & Stellar Ages

The D4000 flux ratio is a well established index of stellar ages (Bruzual 1983 [13], Kauffmann *et al.* 2003 [35]); higher D4000 flux ratios correspond to stellar older galaxies. Therefore we will look into the D4000 histograms of our three galaxy samples to see how many aged systems each sample includes. The sample's D4000 distributions are shown in Figure 3.5. The galaxies of MG1 (black criss-crossed shaded distribution) are distributed symmetricly around the sample's high D4000 mean of 1.75 (solid black line). MG1 is a pure sample of stellar aged systems. Note that more than 85% of the MG1 objects feature a D4000 value > 1.6, and that the remaining 15% have a D4000 > 1.35. The D4000 mean of MG1 and its $1\sigma_{\mathrm{MAD}}$ error are listed also in Table 3.6.
The open grey distribution of Figure 3.5 is the D4000 histogram of MG2. It shows a asymmetric D4000 distribution and features an expanded tail of stellar young objects; about 15% of the MG2 galaxies feature a D4000 value < 1.3, and some of them have even a D4000 < 1.0. The inclusion of these numerous stellar young objects lower the D4000 mean of MG2 too only 1.60 (grey dotted line; see also Table 3.6).
The D4000 spreading of MG3 is represented by the diagonal shaded distribution of Figure 3.5. MG3 shows also an asymmetric D4000 distribution; a tail of stellar young objects is formed, because 15% of the sample's galaxies feature a D4000 < 1.5, and some MG3 objects have even a D4000 value less than 1.2. However, this young galaxy tail of MG3 is less developed than the one of MG2. Therefore, the MG3 sample is also less asymmetric in D4000 space than MG2. As a result, the calculated D4000 mean of MG3 is with 1.70 (black dashed line) closer to the D4000 average of MG1 than to the D4000 mean of MG2 (see also Table 3.6).
The D4000 means of our 3 galaxy samples are distinguishable different from each other due to the different sample distributions in D4000 space (see Tables 3.6 & 3.7 and Figure 3.5). MG1 features always the highest D4000 average and MG2 always the lowest. The average stellar age of MG3 is closer to MG1 than to MG2, but it never reaches the average value of our Hα-selection (MG1). A clear D4000 gap of ~ 0.05 separates the two samples (MG1 & MG3) throughout the observed redshift range.
For lower and mid stellar galaxy ages (D4000 < 1.9) the shapes of the D4000 distributions are different to each other, but for higher stellar ages (D4000 > 1.9) the 3 histograms look alike and cover each other. All 3 samples include the most stellar aged galaxies. Thus, we can see that our applied selection criteria affect and exclude only younger galaxies, stellar old objects remain untouched by them.
We confirm the correctness of the calculated D4000 means by additionally measuring the D4000 flux ratios from the sample's luminosity weighted average spectra (see Figure 3.3). These measured D4000-values (Table 3.7) are consistent with the data listed in Table 3.6. Both methods, calculating the sample's D4000 mean or measuring it from the sample's

average spectrum provide one with consistent D4000 averages. Even the $1\sigma_{\mathrm{MAD}}$ errors of the D4000 averages are consistent with each other.
The Tables 3.6 & 3.7 show that both D4000 means, measured & calculated ones, increase constantly over the entire observed redshift range. This is caused by the higher luminosity limits ($M_{r'}$-cuts) at higher z. As shown by Gallazzi *et al.* 2006 [25], the stellar age of red sequence galaxies increases with luminosity. We find this same effect here in our 3 red sequence samples of MG1, MG2 & MG3; we increase the average luminosity of our red sequences by going to higher redshifts (see Figure 2.1) and observe that the sample's mean stellar ages (indicated by the D4000-averages) increase monotonicly to higher values.
We use the stellar synthesis model of Bruzual & Charlot 2003 [12] to calculate the sample's stellar ages in Gyr based on the D4000 means listed in Tables 3.6 & 3.7. To do so we use the following initial conditions in the stellar synthesis modeling code of Bruzual & Charlot 2003 [12]:

- solar metallicity (Z = 0.2)
- Salpeter IMF (initial mass function)
- only one single stellar burst of zero time length at t = 0
- after star formation ceased only passive galaxy evolution is allowed

According to the NYU Catalog, each galaxy included in MG1, MG2 & MG3 features at least solar metallicity. Since we are only interested in comparing the sample's relative average ages with each other, we do not implement different metallicities or star formation histories among our samples. We do not change metallicity along the red sequences of MG1, MG2 & MG3, we only use solar metallicity for all sample galaxies. The average stellar ages of MG1, MG2 & MG3 in Gyr are listed in the Tables 3.6 & 3.7. The Hα-sample (MG1) is on average the stellar oldest galaxy selection followed by sample MG3. Both samples have an average age greater than 3 Gyr but are separated by at least 0.25 Gyr. MG2 has by far the youngest average stellar age. The age gap between MG2 & MG3 is mostly about 0.5 Gyr, a significant age difference nearly constant throughout $0.05 < z \leq 0.15$. Comparing the age distributions of all three samples one can see that the Hα-selected sample (MG1) features the most uniform & homogeneous selection of stellar old galaxies. Note that the errors on the D4000 means were not implemented in the calculation of the average Gyr ages.
The code of Bruzual & Charlot 2003 [12] has one disadvantage in the use of the D4000 flux ratio as age estimator. For stellar older objects the D4000 value saturates at higher values (D4000 > 1.7). Small changes in D4000 of ~ 0.04 can correspond to age changes of about 0.5 - 1 Gyr. Therefore, small value increases in the D4000 means (~ 0.01) result in a significantly higher galaxy ages (~ 0.25 Gyr older). In Tables 3.6 & 3.7 one can see how the small increases in the D4000 raise the sample's average ages. However, the age gaps between the samples

remain constant and untouched by this effect. Remember that these age increases are based on the sample's higher average luminosities arising from implemented $M_{r'}$-cuts at higher z. Note also that we assume solar metallicity for all red sequence galaxies of the 3 samples. Thus, we have not fully resolved the age-metallicity degeneracy of early-type galaxies found along the red sequence. We have only shown that at a fixed metallicity the more luminous early-type red sequence galaxies are also more likely to feature older stellar populations.

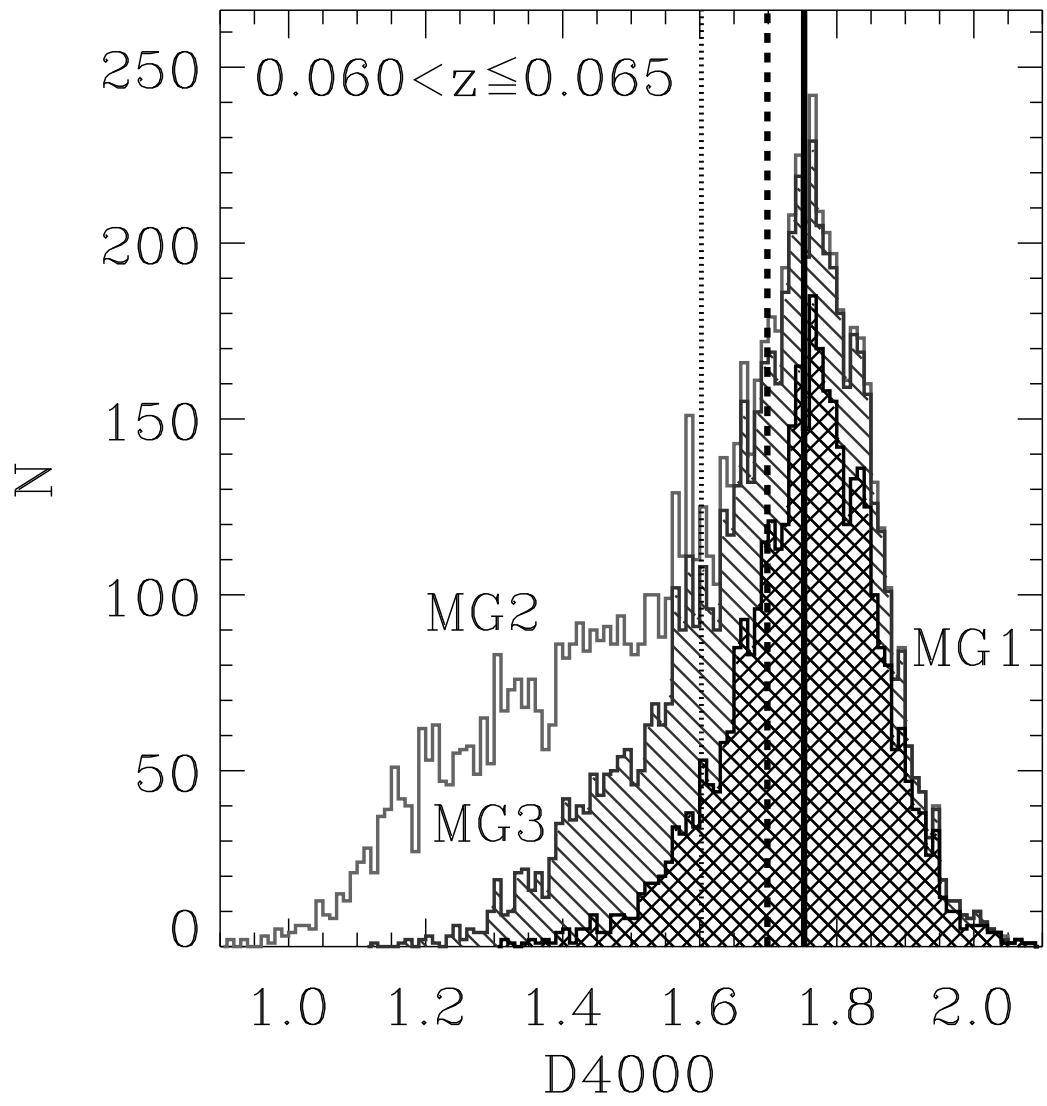

Figure 3.5: The D4000 distribution of MG1 (hatched), MG2 (open) and MG3 (diagonal shaded). The average D4000 value of each sample is indicated by the solid black (MG1), dashed black (MG2), and dotted grey (MG3) lines. MG1 has the highest average D4000, slightly higher than the one of MG3 (see Table 3.6). MG1's distribution is symmetric around its D4000 mean. The other two samples feature a long declining tail towards lower D4000 values, this corresponds to an inclusion of younger galaxies.

Table 3.6: *Ages from Median D4000: MG1, MG2, MG3*[a]

$\triangle z$	$\langle$D4000$\rangle_{\mathrm{MG1}}$[b]	$\langle$Age$\rangle_{\mathrm{MG1}}$[c]	$\langle$D4000$\rangle_{\mathrm{MG2}}$[b]	$\langle$Age$\rangle_{\mathrm{MG2}}$[c]	$\langle$D4000$\rangle_{\mathrm{MG3}}$[b]	$\langle$Age$\rangle_{\mathrm{MG3}}$[c]
$0.050 < z \leq 0.055$	1.74 ±0.11	3.25	1.58 ±0.23	2.10	1.69 ±0.14	3.00
$0.055 < z \leq 0.060$	1.75 ±0.11	3.50	1.59 ±0.22	2.20	1.70 ±0.14	3.00
$0.060 < z \leq 0.065$	1.75 ±0.10	3.50	1.60 ±0.21	2.20	1.70 ±0.14	3.00
$0.065 < z \leq 0.070$	1.75 ±0.10	3.50	1.61 ±0.21	2.30	1.70 ±0.13	3.00
$0.070 < z \leq 0.075$	1.76 ±0.09	3.50	1.62 ±0.19	2.40	1.70 ±0.13	3.00
$0.075 < z \leq 0.080$	1.76 ±0.09	3.75	1.63 ±0.19	2.50	1.72 ±0.12	3.00
$0.080 < z \leq 0.085$	1.76 ±0.09	3.75	1.64 ±0.19	2.50	1.71 ±0.12	3.00
$0.085 < z \leq 0.090$	1.77 ±0.09	3.75	1.64 ±0.18	2.60	1.72 ±0.12	3.00
$0.090 < z \leq 0.095$	1.77 ±0.09	3.75	1.64 ±0.18	2.60	1.72 ±0.12	3.00
$0.095 < z \leq 0.100$	1.77 ±0.08	4.00	1.64 ±0.18	2.60	1.72 ±0.12	3.00
$0.100 < z \leq 0.105$	1.77 ±0.09	4.00	1.64 ±0.19	2.60	1.72 ±0.12	3.00
$0.105 < z \leq 0.110$	1.77 ±0.09	4.00	1.64 ±0.18	2.60	1.72 ±0.12	3.00
$0.110 < z \leq 0.115$	1.78 ±0.09	4.00	1.65 ±0.18	2.60	1.73 ±0.12	3.25
$0.115 < z \leq 0.120$	1.78 ±0.09	4.00	1.65 ±0.18	2.75	1.73 ±0.12	3.25
$0.120 < z \leq 0.125$	1.78 ±0.09	4.00	1.65 ±0.18	2.75	1.73 ±0.12	3.25
$0.125 < z \leq 0.130$	1.78 ±0.08	4.00	1.66 ±0.18	2.75	1.74 ±0.11	3.25
$0.130 < z \leq 0.135$	1.79 ±0.08	4.25	1.67 ±0.17	2.75	1.74 ±0.11	3.25
$0.135 < z \leq 0.140$	1.79 ±0.08	4.25	1.68 ±0.17	2.75	1.75 ±0.11	3.50
$0.140 < z \leq 0.145$	1.80 ±0.08	4.25	1.68 ±0.16	2.75	1.76 ±0.11	3.75
$0.145 < z \leq 0.150$	1.80 ±0.08	4.50	1.69 ±0.17	3.00	1.77 ±0.11	3.75

[a] We use the stellar synthesis model code of Bruzual & Charlot 2003 [12] with solar metallicity (Z = 0.2) and the Padova stellar evolution track to calculate an age estimation. The Salpeter IMF was used in the calculation of the ages listed in this table.

[b] The mean D4000-values of MG1, MG2, and MG3 (see Fig. 3.5).

[c] The age derived from the sample's mean D4000-values.

Table 3.7: *Ages from D4000 of Averaged Spectra: MG1, MG2, MG3*[a]

$\triangle z$	$D4000_{MG1}$[b]	$\langle Age\rangle_{MG1}$[c]	$D4000_{MG2}$[b]	$\langle Age\rangle_{MG2}$[c]	$D4000_{MG3}$[b]	$\langle Age\rangle_{MG3}$[c]
$0.050 < z \leq 0.055$	1.72 ±0.11	3.00	1.51 ±0.24	1.27	1.67 ±0.14	2.75
$0.055 < z \leq 0.060$	1.73 ±0.10	3.25	1.52 ±0.22	1.13	1.67 ±0.14	2.75
$0.060 < z \leq 0.065$	1.73 ±0.10	3.25	1.54 ±0.22	1.70	1.68 ±0.14	2.75
$0.065 < z \leq 0.070$	1.74 ±0.10	3.25	1.55 ±0.21	1.80	1.68 ±0.13	2.75
$0.070 < z \leq 0.075$	1.74 ±0.09	3.25	1.57 ±0.19	1.90	1.69 ±0.13	3.00
$0.075 < z \leq 0.080$	1.75 ±0.09	3.50	1.58 ±0.19	2.10	1.70 ±0.12	3.00
$0.080 < z \leq 0.085$	1.75 ±0.09	3.50	1.59 ±0.19	2.10	1.70 ±0.12	3.00
$0.085 < z \leq 0.090$	1.75 ±0.09	3.50	1.60 ±0.18	2.20	1.71 ±0.12	3.00
$0.090 < z \leq 0.095$	1.76 ±0.09	3.50	1.59 ±0.18	2.20	1.71 ±0.12	3.00
$0.095 < z \leq 0.100$	1.76 ±0.08	3.75	1.60 ±0.18	2.20	1.71 ±0.12	3.00
$0.100 < z \leq 0.105$	1.76 ±0.09	3.75	1.60 ±0.19	2.20	1.70 ±0.12	3.00
$0.105 < z \leq 0.110$	1.76 ±0.09	3.75	1.61 ±0.18	2.30	1.71 ±0.12	3.00
$0.110 < z \leq 0.115$	1.76 ±0.09	3.75	1.61 ±0.18	2.30	1.72 ±0.12	3.00
$0.115 < z \leq 0.120$	1.77 ±0.09	3.75	1.61 ±0.18	2.30	1.72 ±0.12	3.00
$0.120 < z \leq 0.125$	1.77 ±0.09	3.75	1.61 ±0.18	2.30	1.72 ±0.12	3.00
$0.125 < z \leq 0.130$	1.77 ±0.08	4.00	1.62 ±0.18	2.40	1.72 ±0.11	3.00
$0.130 < z \leq 0.135$	1.78 ±0.08	4.00	1.63 ±0.17	2.50	1.73 ±0.11	3.25
$0.135 < z \leq 0.140$	1.78 ±0.08	4.00	1.64 ±0.17	2.50	1.74 ±0.11	3.25
$0.140 < z \leq 0.145$	1.78 ±0.08	4.25	1.65 ±0.16	2.60	1.75 ±0.11	3.50
$0.145 < z \leq 0.150$	1.79 ±0.08	4.25	1.65 ±0.17	2.75	1.75 ±0.11	3.50

[a] We use the stellar synthesis model code of Bruzual & Charlot 2003 [12] with solar metallicity (Z = 0.2) and the Padova stellar evolution track to calculate an age estimation. The Salpeter IMF was used in the calculation of the ages listed in this table.

[b] The measured D4000 values of the sample's average spectrum (see Fig. 3.3).

[c] The ages derived from the D4000-values of the sample's average spectrum.

3.6 MG Samples: Sérsic index vs. D4000

To shed some light on the correlation between the stellar age and morphology of galaxies one can plot the D4000 flux ratio (stellar age) against the the Sérsic index n. Thus we will see how strong the correlation between stellar age (D4000) and morphology (Sérsic n) is in detail. We are then also able to see which selection criteria, photometric or spectroscopic one, correlates the most with the stellar age of galaxies.
To get an idea about the Sérsic n vs. D4000 parameter space we plot all galaxies inside the $0.06 < z \leq 0.065$ redshift bin in the Sérsic n vs. D4000 diagram of Figure 3.6 (lower right panel). The galaxies are distributed bimodal in this parameter space. The stellar younger late-type systems are concentrated in the lower left corner of this diagram ($n < 2$ & D4000 < 1.4) and the stellar older early-type galaxies occupy the right mid part of it ($n > 2$ & D4000 > 1.6). This bimodal parameter space distribution is comparable with the bimodal galaxy distribution one expects to see in colour-magnitude diagram ("blue cloud" and "red sequence"). However, nearly the entire parameter space is covered by galaxies and no correlation between age (D4000 index) and morphology (Sérsic index) or an occupation limitation caused by these values is visible. The galaxy overdensity at Sérsic $n \sim 6$ is based on the Sérsic threshold of the NYU VAGC. Every galaxy measured with a Sérsic $n > 6$ gets a listed Sérsic index of $n = 6$ in this catalogue. The blue dashed line at Sérsic $n = 2$ is the Sérsic limit used to discriminate between early- and late-type objects (see Table 2.2).
The Sérsic n vs. D4000 diagram of MG1 is drawn in the upper left panel of Figure 3.6. The sample's galaxies occupy only a limited area of this parameter space. About 99% of the MG1 galaxies have Sérsic $n > 2$ and are therefore early-type objects, although we never selected by Sérsic n in this sample. The galaxies of MG1 are distributed over the same Sérsic n range like the galaxies of MG2 & MG3 (Sérsic $n > 2$). The upper left diagram of Figure 3.6 shows also that all sample galaxies of MG1 are distributed symmetricly in D4000-space and are concentrated towards higher D4000 values (D4000 > 1.5).
The upper right panel of Figure 3.6 shows the MG2 sample. This sample is distributed over the entire parameter space and shows no clear correlation between Sérsic n & D4000. Note, that the MG2 sample occupies the same Sérsic n range like MG1, but unlike our Hα-selected sample the MG2 selection spreads over the entire drawn D4000 space.
The MG3 sample is presented in the lower left panel of Figure 3.6. MG3 is less extended in Sérsic n vs. D4000 space than MG2 due to the colour-cut exclusion of younger blue early-type galaxies. However, even by colour-cutting we could not minimise the D4000 spreading significantly. The MG3 galaxies are still spread over a larger D4000 range, much larger than MG1. Therefore we conclude that Sérsic index n & colour are not as strict in selecting stellar old early-type galaxies than the Hα-absorption criterion alone.

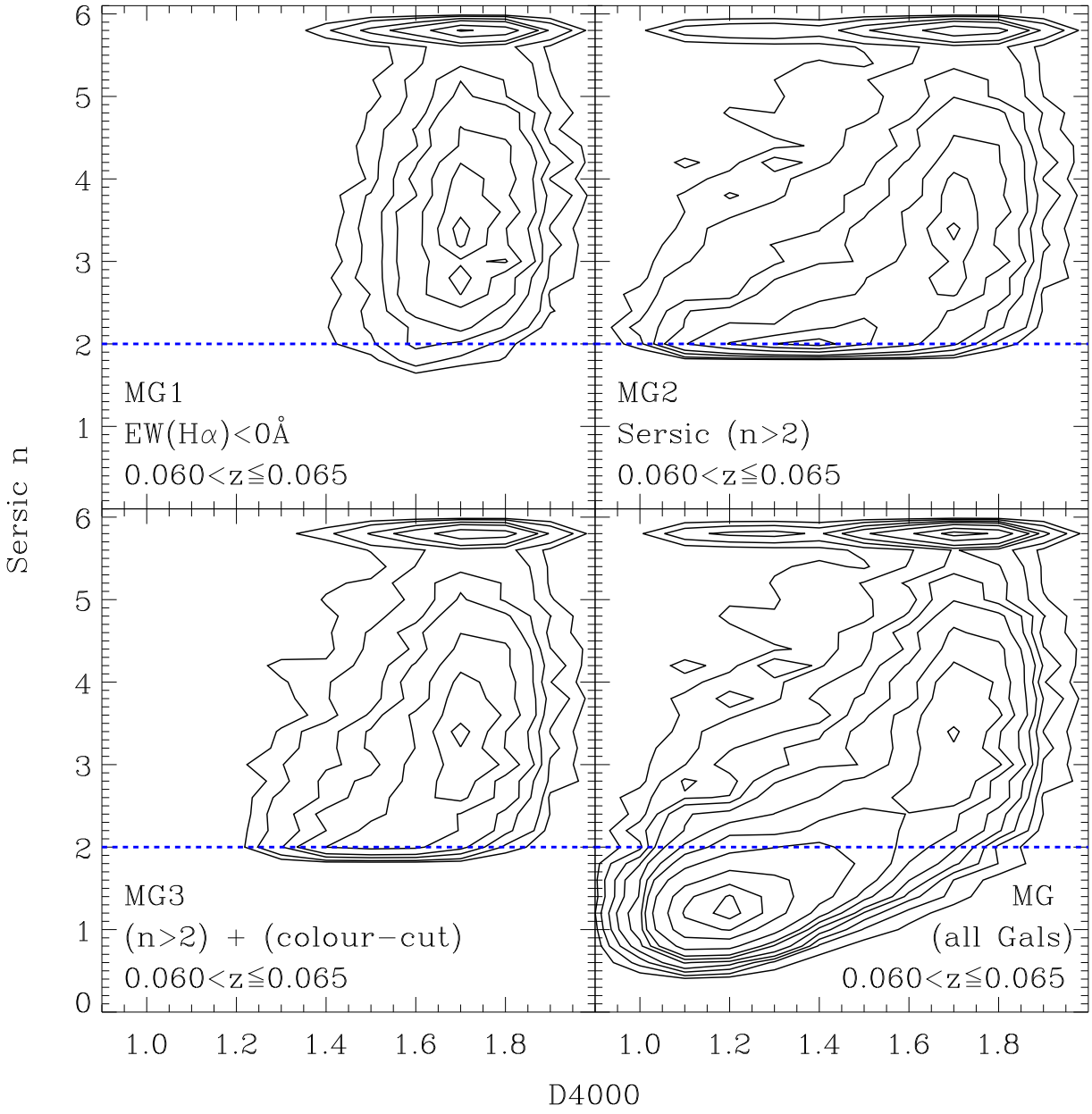

Figure 3.6: The distribution in Sérsic n and D4000 space for MG1 (upper left), MG2 (upper right), MG3 (bottom left), and all galaxies (bottom right). All distributions are for the same redshift range. The dashed line inside each panel represents the parameter cut of Sérsic index $n = 2$ used in the selection of MG2 & MG3. The overdensity at Sérsic $n \sim 6$ is based on the NYU catalog's threshold in the calculation of the Sérsic index n where every galaxy with n > 6 gets a listed Sérsic index of $n = 6$. MG1 (the Hα sample) consists nearly exclusively of bulge dominated galaxies with a Sérsic index $n > 2$.

3.7 Results from the Luminous Galaxy Samples

As we have seen in Section 3.4 that it is possible to minimise a sample's contamination of star forming galaxies by applying higher luminosity limits ($M_{r'}$-cuts). We will now use a high luminosity limit of $M_{r'}$ = -21.0 constant in redshift space. This enable us to study the selection effects of our applied criteria regarding the brightest and therefore also more likely passive galaxies within $0.05 < z \leq 0.15$. In that manner we can repeat our previous analysis on a galaxy catalog populated only with high signal-to-noise objects.
Using the constant $M_{r'}$ = -21.0 limit as an additional selection criterion inside the redshift binned BPT-diagnostic of MG2 (Table 3.4) results in constant and redshift independent sample fractions of SF, AGN & AGN/SF galaxies. Testing these fractions against redshift by calculating the Spearman's correlation coefficient confirms that there is no significant correlation between these galaxy types (SF, AGN & AGN/SF) and redshift z. Based on the constant AGN-fraction we conclude that there is no indication of significant galaxy evolution in the redshift range of $0.05 < z \leq 0.15$. Therefore, we waive to redshift bin the Luminous Galaxy (LG) samples.
The selection criteria and sizes (N_{gal}) of the 3 Luminous Galaxy Samples can be found in Table 2.3. Note, since we are now covering a more extended redshift range ($\triangle z = 0.1$) we will use rest frame colour and absolute magnitudes in our further analysis.

3.7.1 Luminous Galaxy Samples: Colour-magnitude relation

The colour-magnitude diagrams of LG1, LG2 & LG3 are shown in Figure 3.7, the data of these plots are listed in Table 3.8. The CMRs of LG1, LG2 & LG3 are in good agreement to each other. LG2 & LG3 feature an identical CMR, and the CMR of LG1 shows only a slight offset to them. Determine the 3 CMR slopes of these 3 samples (LG1, LG2 & LG3) we will not notice any difference to the earlier found CMR slopes (MG samples). The CMR normalisation n between the LG and MG samples is different due to the change from apparent to absolute colours & magnitudes. The red sequence scatter differs also between the LG and MG samples differs; MG1, MG2 & MG3 have a scatter σ_{MAD} of about 0.05, 0.1 & 0.06 (respectively), LG1, LG2 & LG3 show only a σ_{MAD} of about 0.035, 0.069 & 0.043, 1/3 lower in value. The scatter shrinking is based on the now used K-corrected absolute magnitudes of the NYU VAGC. We have seen, *e.g.* in Table 3.2, that an apparent red sequence (apparent colour & magnitude) features always a redshift dependent colour range which stretches with z (K-correction effect on the colour; see also Hogg *et al.* 2002 [30]). A rest-frame red sequence (*e.g.* LG1) is not subject to this z dependent effect, its scatter in colour is smaller due to the K-corrections on the galaxy's colour.
The tighter colour distribution of LG1 & LG2 is also visible in Figure 3.8, it shows the colour residuals $\triangle(g'-r')$ of LG1 & LG2. LG1 has a symmetric shape around its fitted CMR (black

solid line) and a very low scatter ($\sigma_{\rm MAD} = 0.035$). LG2 on the other hand shows a higher scatter of $\sigma_{\rm MAD} \simeq 0.07$ caused by its tail of blue galaxies. Note that the blue tail in here is less extended than the one of MG2 (Figure 3.2). The plotted red dashed line is the $3\sigma_{\rm MAD}$ of LG1 (colour-cut); about 24% of the LG2 objects have $\triangle(g' - r') <$ -$3\sigma_{\rm MAD}$.
Comparing the Figures 3.2 & 3.8 with each other suggests that the LG1 & LG2 samples are more peaked in $\triangle(g' - r')$ space than their cousin samples of MG1 & MG2. These more developed sample peaks in $\triangle(g' - r')$ explain why the $\sigma_{\rm MAD}$ scatter value is lower in the LG samples than in the MG ones.

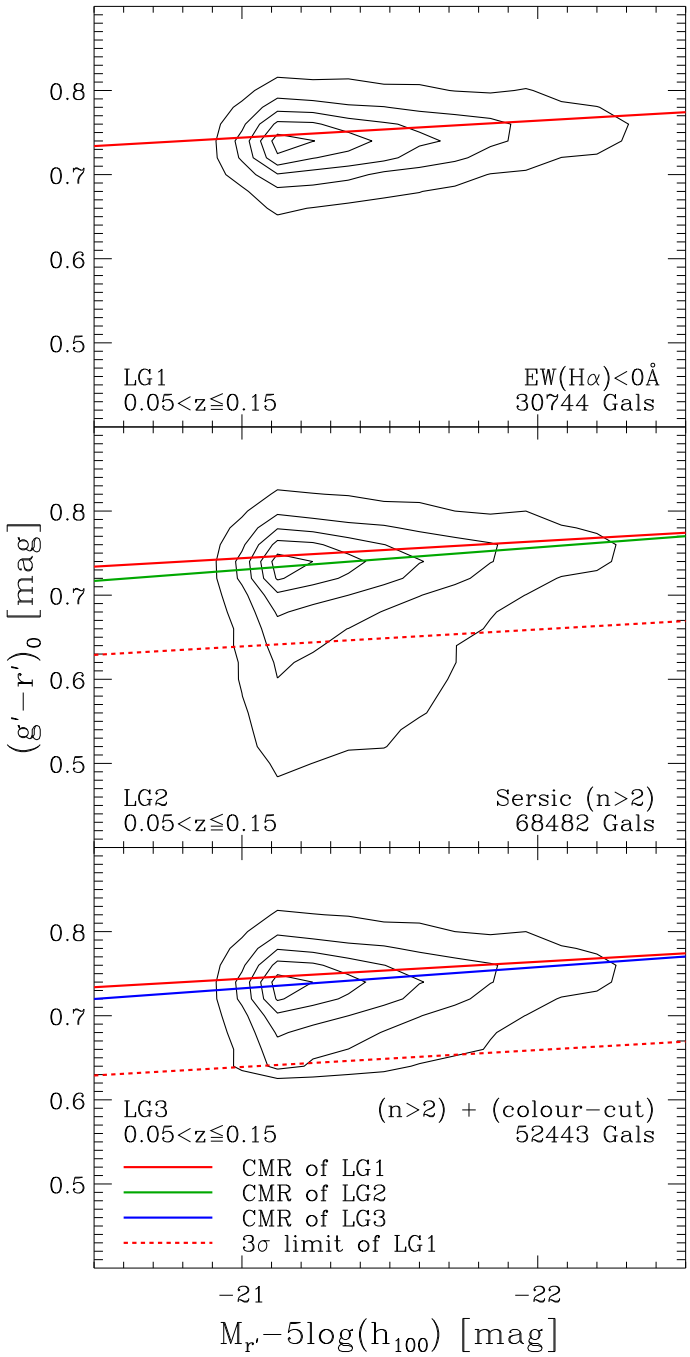

Figure 3.7: The rest-frame colour-magnitude diagrams of LG1 (Hα passive), LG2 (Sérsic $n > 2$), and LG3 (Sérsic $n > 2$ + colour-cut). All galaxies have $M_{r'}$ < -21.0 and a redshift of $0.05 < z \leq 0.15$ (see Fig. 2.1). The drawn solid lines are the sigma-clipped least squares fits of LG1 (red), LG2 (green), and LG3 (blue). The dotted red line is the $3\sigma_{\mathrm{MAD}}$ limit of LG1 ($3\sigma_{\mathrm{MAD}} = 0.1$). Plotting the galaxy samples our 3 selection criteria in rest-frame colour/magnitude system results in a tighter red sequence than plotting the samples in apparent colour/magnitude system (see Figure 3.1). The tighter red sequence is caused by the K-correction in colour of each sample's galaxy. The Hα-criterion provides one with the purest red sequence sample.

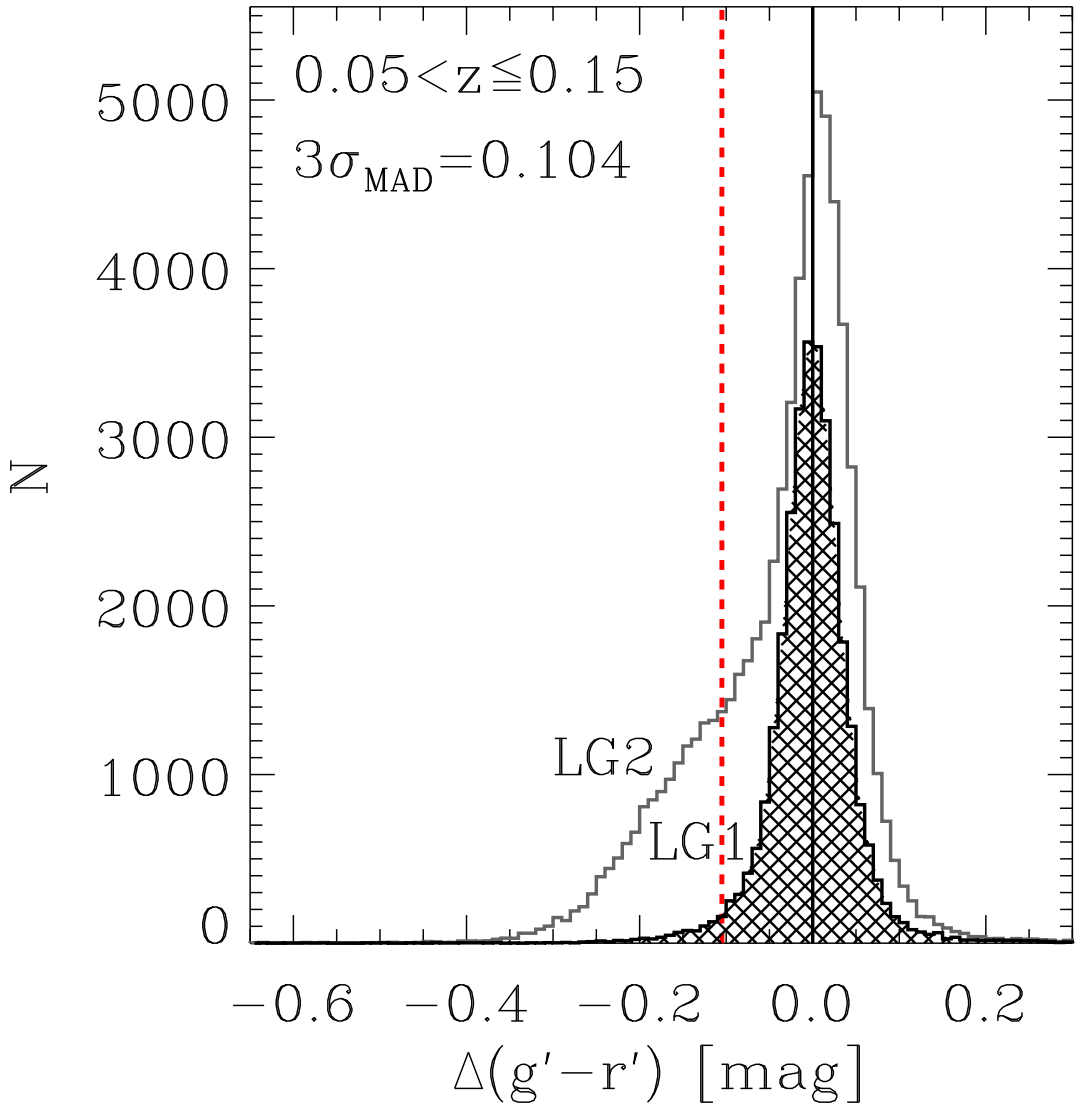

Figure 3.8: he histogram of the rest-frame colour residuals $\triangle(g' - r')$ of LG1 (hatched)& LG2 (open). The black solid line represents each sample's CMR, and the dashed line is the $3\sigma_{\rm MAD}$ of the LG1 sample (colour-cut). LG1 shows a very peaked colour distribution that is symmetricly around its CMR. The colour residual histograms of both samples (LG1 & LG2) are tighter and more peaked than the apparent colour residual histograms of MG1 & MG2 (see Figure 3.2).

Table 3.8: *Colour-magnitude relations: LG1, LG2, LG3*

Sample	$\triangle$z	f(N_{gal})[a]	$m \pm\sigma_m$[b]	$n \pm\sigma_n$[b]	$\sigma_{\rm MAD}[\triangle(g'-r')]$[c]
LG1	$0.05 < z \leq 0.15$	37.4% (30,744)	-0.020 $\pm$0.016	0.32 $\pm$0.006	0.034 $\pm 5.3{*}10^{-5}$
LG2	$0.05 < z \leq 0.15$	83.3% (68,482)	-0.026 $\pm$0.013	0.17 $\pm$0.004	0.069 $\pm 8.5{*}10^{-4}$
LG3	$0.05 < z \leq 0.15$	63.8% (52,447)	-0.025 $\pm$0.013	0.20 $\pm$0.004	0.044 $\pm 4.3{*}10^{-5}$

[a] The fraction of sample galaxies is calculated with respect to total galaxy number of the LG sample (82,171 galaxies). The value in parentheses is the selected number of galaxies (see Table 2.1).

[b] The slope (m) and normalization (n) of the linear colour-magnitude relation $(g'-r') = n + mr$ and its 1σ errors.

[c] The $1\sigma_{\rm MAD}$ of the colour residual's distribution $\triangle(g'-r')$ and its error. The error was calculated using the Jack-knife resampling method (Miller 1974 [40]).

3.7.2 LG Samples: Fractions

LG1 includes with $\sim 37\%$ of the luminous galaxies the fewest objects, and LG3 with $\sim 83\%$ the most luminous galaxies. Nearly all LG1 galaxies are also inlcuded inside LG2 & LG3; 99% of the LG1 galaxies can be found in LG2, and 97% of them are also located inside LG3. That means, that LG2 consist to $\sim 44\%$ of Hα-passive galaxies, and LG3 is made up of $\sim$ 57% by Hα-passive objects. About 76% of the LG2 galaxies lie above the colour-cut and are included in LG3. These fraction values are consistent with the values found in the earlier samples of MG1, MG2 & MG3 (see Section 3.2).

3.7.3 LG Samples: Spectral properties

The luminosity weighted average spectra of LG1, LG2 & LG3 are presented in Figure 3.9. All 3 spectra feature a SED continuum shape of an early-type galaxy. The sample's 4000Å-breaks are with a measured D4000 flux ratio of 1.79 (LG1), 1.65 (LG2) & 1.74 (LG3) highly elevated. The spectra of LG1 & LG3 do not differ in their overall properties from each other (4000Å-break, SED continuum shape). Detailed differences between these two samples are only detectable if one looks at the emissions of Hα, N[II] & O[II]; the LG3 spectrum shows small emission in all these lines, LG1 on the other hand does not show any emission in all 3 lines. The LG1 spectrum is totally passive with deep absorption lines in Hα & Hβ.
The spectra of LG2 & LG3 show both emission in Hα & N[II]. The equal line emissions of in both lines suggest that the net active emission in both samples is dominated by AGN galaxies.
Comparing these 3 average spectra (Figure 3.9) with the earlier presented ones (Figure 3.3) points out, that only the spectra of the Sérsic selections (MG2 & LG2) differ significantly from each other. MG2 shows strong emissions in Hα, Hβ and O[II], but LG2 features only small and equal emission in these 3 lines (AGN emission). The only selection difference between these two Sérsic samples responsible for this change is the luminosity limit in $M_{r'}$. Higher luminosity limits will prevent the sample inclusion of star forming galaxies, but these higher limits cannot achieve the same for AGN galaxies. AGNs can make it into the sample, because they are on average brighter than star formung galaxies (see also Table 3.4).

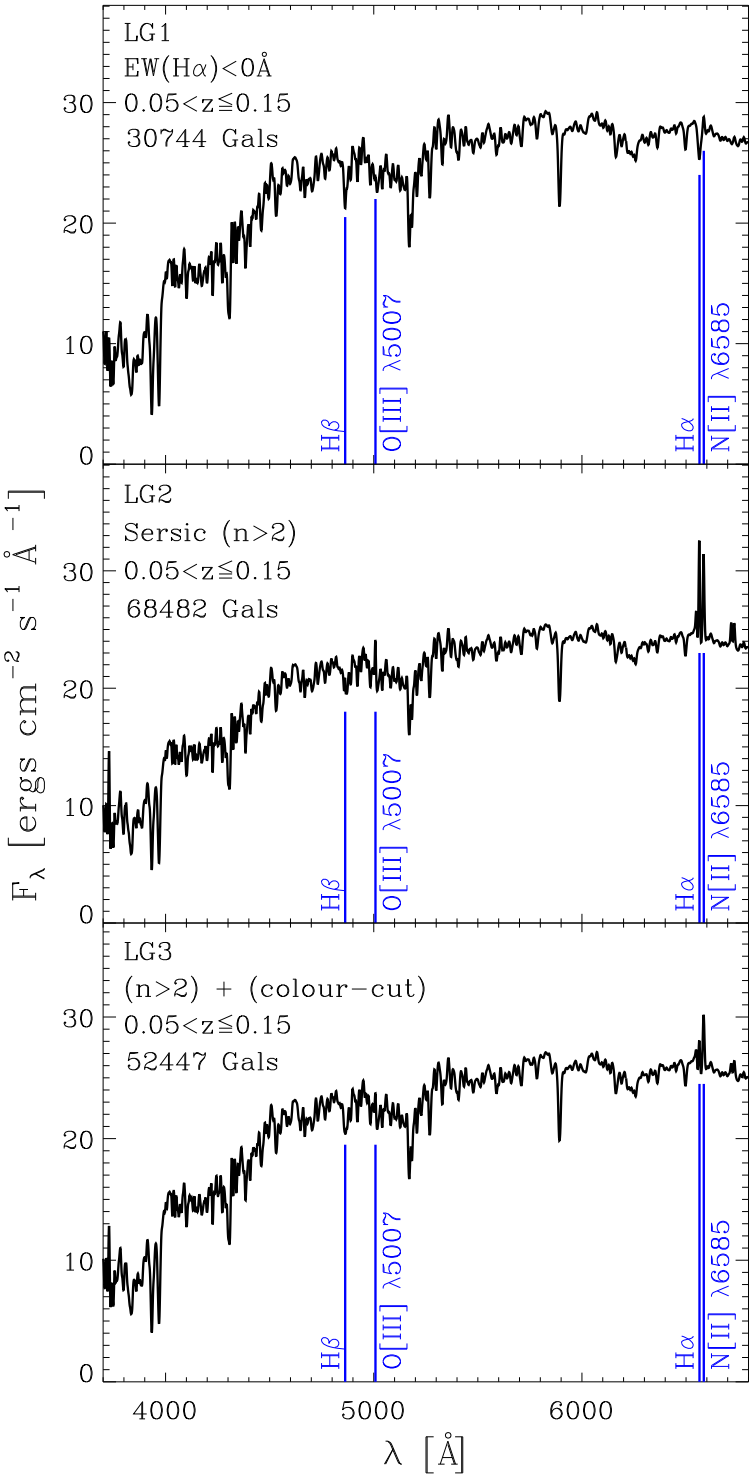

Figure 3.9: The luminosity weighted average spectra of LG1 (top panel), LG2 (mid panel) & LG3 (bottom panel). All 3 spectra feature an early-type SED continuum, that is in contrast to Figure 3.3 where only MG1 & MG3 show early-type character. The difference between the average spectra of MG2 & LG2 are based on the different luminosity limits inside these two samples. The higher luminosity limit ($M_{r'}$-cut) in LG2 excludes most starforming galaxies.

3.7.4 LG Samples: AGN vs. Star Formation

BPT-diagnostic can quantify the AGN component of our luminous galaxy samples. The BPT-diagrams of LG2 & LG3 are shown in Figure 3.10, and their data are listed in Table 3.9. Note again, that we cannot use BPT-diagnostic for the Hα-selected sample of LG1, because the analysis requires emission in Hα. LG2 & LG3 feature only a small fraction of active emission line galaxies; 14% of the LG2 galaxies show simultaneous emission in Hα, Hβ, N[II] & O[III]. Even lower is the active galaxy fraction of LG3, only 5% of this sample show emission in all these 4 lines. The two BPT-diagrams of LG2 & LG3 show, that the fraction of starforming galaxies (SF) is very low in both samples. LG2, the left panel of Figure 3.10, includes only 2.9% starforming galaxies, and the SF fraction of LG3 (right panel) is with 0.3% close to 0. The AGN and AGN/SF galaxies on the other hand dominate the line emissions in both samples. Note that we can reduce the number of AGN and AGN/SF galaxies inside an early-type selection significantly by using a colour-cut, but doing so we cannot prevent the inclusion of AGN and AGN/SF galaxies in general. The Hα-criterion achieves this without problems.
It seems that our photometric selection criteria of Sérsic index n and colour-cut are more effective identifying passive galaxies at higher luminosities than they were at lower luminosities. They include less starforming objects into the LG2 & LG3 samples than they do for MG2 & MG3, the galaxy samples with lower luminosity limits. But note that this improvement is mainly based on the higher luminosity limit itself and not on the actual photometric selection criteria. Pre-selecting galaxies by applying higher luminosity limits will prevent the sample inclusion of star forming and some AGN/SF galaxies. However, even in the high luminosity case, the Hα-selection (LG1) remains the best galaxy sample of passive non-starforming red sequence objects. The LG1 sample shows no indication of star forming or AGN activity and is the purest sample of passive galaxies.

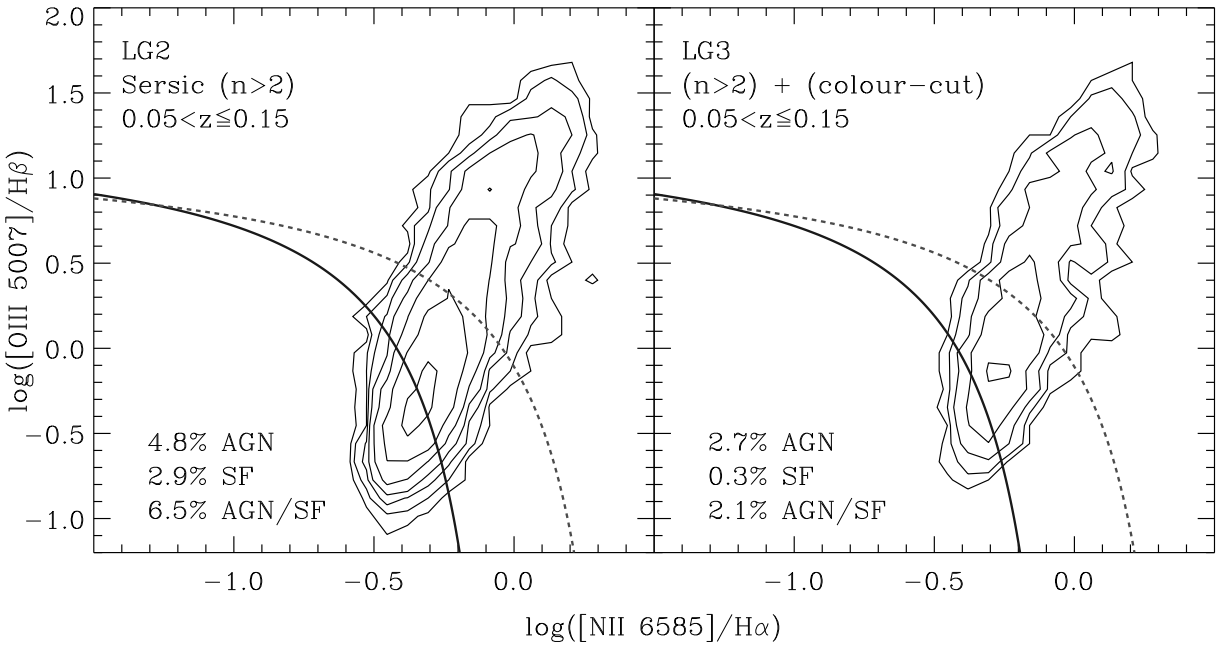

Figure 3.10: The BPT-diagrams of the active galaxies in LG2 (left panel) and LG3 (right panel). The black solid line represents the separation curve of Kauffmann *et al.* 2003 [34] and the grey dashed line the separation curve of Kewley *et al.* 2001 [38]. This plot is comparable with the one shown in Figure 3.4, but the fraction of SF and AGN/SF galaxies is lower in the samples of LG2 & LG3 than in MG2 & MG3. This is due to the higher luminosity cut in the LG sample.

Table 3.9: *AGN fraction: LG2, LG3*

Sample	$\triangle$z	f($N_{\rm active}$)	f($N_{\rm AGN}$)[a]	f($N_{\rm AGN/SF}$)[b]	f($N_{\rm SF}$)[c]
LG2	$0.05 < z \leq 0.15$	14.2% (9,695)	4.8% (3,274)	6.5% (4,467)	2.9% (1,954)
LG3	$0.05 < z \leq 0.15$	5.2% (2,703)	2.7% (1,415)	2.1% (1,121)	0.3% (167)

[a] The fraction of pure AGN dominated galaxies identified by the separation line of Kewley *et al.* 2001 [38] (see Fig. 3.10). The value in parentheses is the selected number of galaxies.

[b] The fraction of mixed AGN/starforming galaxies identified by the separation lines of Kauffmann *et al.* 2003 [34] and Kewley *et al.* 2001 [38] (see Fig. 3.10). The value in parentheses is the selected number of galaxies.

[c] The fraction of star-forming galaxies identified by the separation line of Kauffmann *et al.* 2003 [34] (see Fig. 3.10). The value in parentheses is the selected number of galaxies.

3.8 LG Samples: D4000 distribution & Stellar Ages

The D4000 distributions of LG1, LG2 & LG3 are plotted in Figure 3.11. LG2 (open grey distribution) is the most extended D4000 distribution. Its developed tail of stellar younger galaxies is responsible for the asymmetric D4000 distribution and lowers the sample's D4000 mean too only 1.69 (grey dotted line).
LG3 includes less younger galaxies than LG2, therefore it has a higher D4000 mean of 1.75 (black dashed line in Figure 3.11). The LG3 sample features also a tail of young galaxies (less developed compared to LG2) which causes the sample's asymmetric D4000 distribution.
Only the LG1 sample (black criss-crossed distribution in Figure 3.11), our Hα-selected galaxy sample, shows a symmetric D4000 distribution around the its high D4000 average of 1.80 (black solid line).
To confirm the correctness of each sample's calculated D4000 mean, we measured the D4000 flux ratios of the sample's 3 average spectra shown in Figure 3.9. We find no disagreements between the D4000 averages. Calculating the D4000 average from the sample itself or measuring it from the sample's average spectrum provide one with consistent values.
Like in Section 3.5, we use the code of Bruzual & Charlot 2003 [12] to estimate the sample's median age based on their D4000 means. We use the same parameters mentioned in Section 3.5 to calculate the average ages. Table 3.10 lists the sample's D4000 means and their connected stellar median ages in Gyr. The LG1 sample has with 5 Gyr the highest stellar age, and the Sérsic selected morphology sample of LG2 with 3 Gyr the lowest age.
The listed average ages and D4000 means of the LG1, LG2 & LG3 are consistent with the results found in higher redshift bins ($z > 0.13$) of the MG samples (Tables 3.6 & 3.7). Even the age differences between the galaxy samples are of the same magnitude. Comparing the ages of the LG samples with the age values listed in the lowest redshift bins of the MG samples shows a significant difference: the three MG samples are much younger there. By this comparison we can now finally conclude that stellar age judged by the D4000 flux ratio is luminosity dependent; more luminous galaxies are also likely to be older in luminosity weighted stellar age.

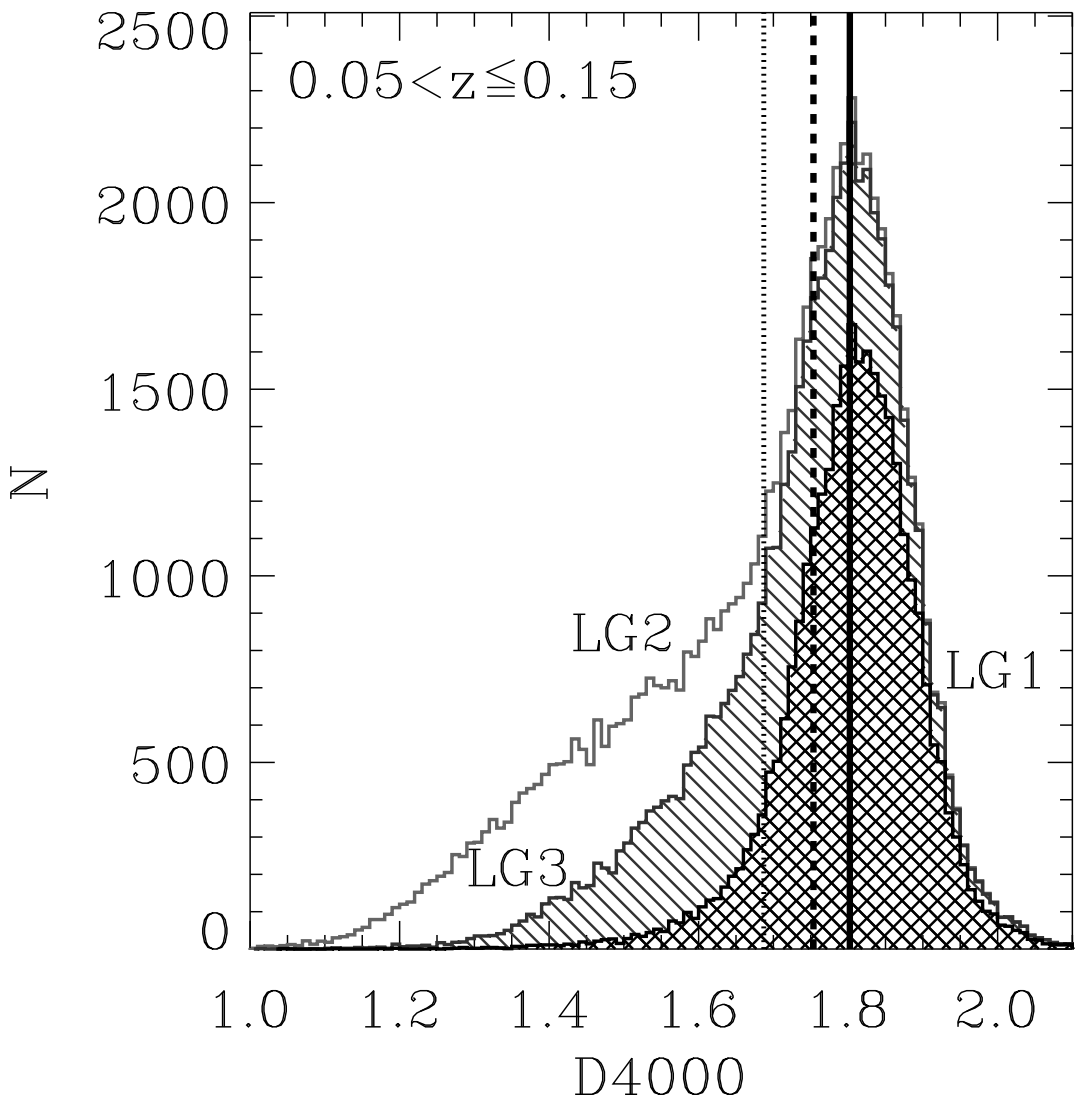

Figure 3.11: The D4000 distribution of LG1 (hatched), LG2 (open) & LG3 (diagonal shaded). The Luminous Galaxy samples have both a narrower and more peaked distribution in D4000 than the Main Galaxy samples (see Figure 3.5) because their higher luminosity limit excludes the fainter galaxies which also tend to be younger.

Table 3.10: *Ages for LG1, LG2, LG3*[a]

Sample	$\triangle z$	$(\mathrm{D4000})_{\mathrm{LG1}}$	$\langle\mathrm{Age}\rangle_{\mathrm{LG1}}$	$(\mathrm{D4000})_{\mathrm{LG2}}$	$\langle\mathrm{Age}\rangle_{\mathrm{LG2}}$	$(\mathrm{D4000})_{\mathrm{LG3}}$	$\langle\mathrm{Age}\rangle_{\mathrm{LG3}}$
D4000 distribution (Figure 3.11)	$0.05 < z \leq 0.15$	1.80 $\pm$0.08	4.50	1.69 $\pm$0.16	3.00	1.75 $\pm$0.11	3.50
Average spectrum (Figure 3.9)	$0.05 < z \leq 0.15$	1.79 $\pm$0.08	4.25	1.65 $\pm$0.16	2.75	1.74 $\pm$0.11	3.25

[a] We use the stellar synthesis model code of Bruzual & Charlot 2003 [12] with solar metallicity (Z = 0.2), Salpeter IMF, and the Padova stellar evolution track to estimate an age.

3.9 LG Samples: Sérsic index vs. D4000

In Figure 3.12 one can see how well the D4000 age estimator and the morphology parameter of Sérsic n are correlating in the samples of high luminous galaxies. The 4 diagram panels of this figure are consistent and look identical with the 4 plots presented in Figure 3.6. The luminous galaxies in $0.05< z \leq 0.15$ are distributed bimodally in Sérsic n vs. D4000 space (lower right panel of Figure 3.12), like it is the case for less luminous galaxies (see lower right panel of Figure 3.6).
The LG2 sample (upper right panel of Figure 3.12) includes the highest fraction of stellar young galaxies and is therefore broadly distributed in the Sérsic n vs. D4000 parameter space. No correlation between Sérsic n & D4000 is visible in this sample. This is similar to the results found in sample MG2 (see Figure 3.6).
The LG3 galaxies (lower left panel of Figure 3.12) occupy a smaller Sérsic n vs. D4000 space than the objects of LG2, because the stellar youngest early-type objects are excluded by the colour-cut. However, this reduction is not as effective as selecting stellar old galaxies by Hα.
The LG1 sample (upper left panel) occupies the fewest parameter space. It also shows the best correlation between Sérsic n & D4000. Nearly all LG1 objects have a D4000 > 1.5 and nearly all of them feature a Sérsic $n > 2$. It is the purest and best sample of stellar old red sequence galaxies.

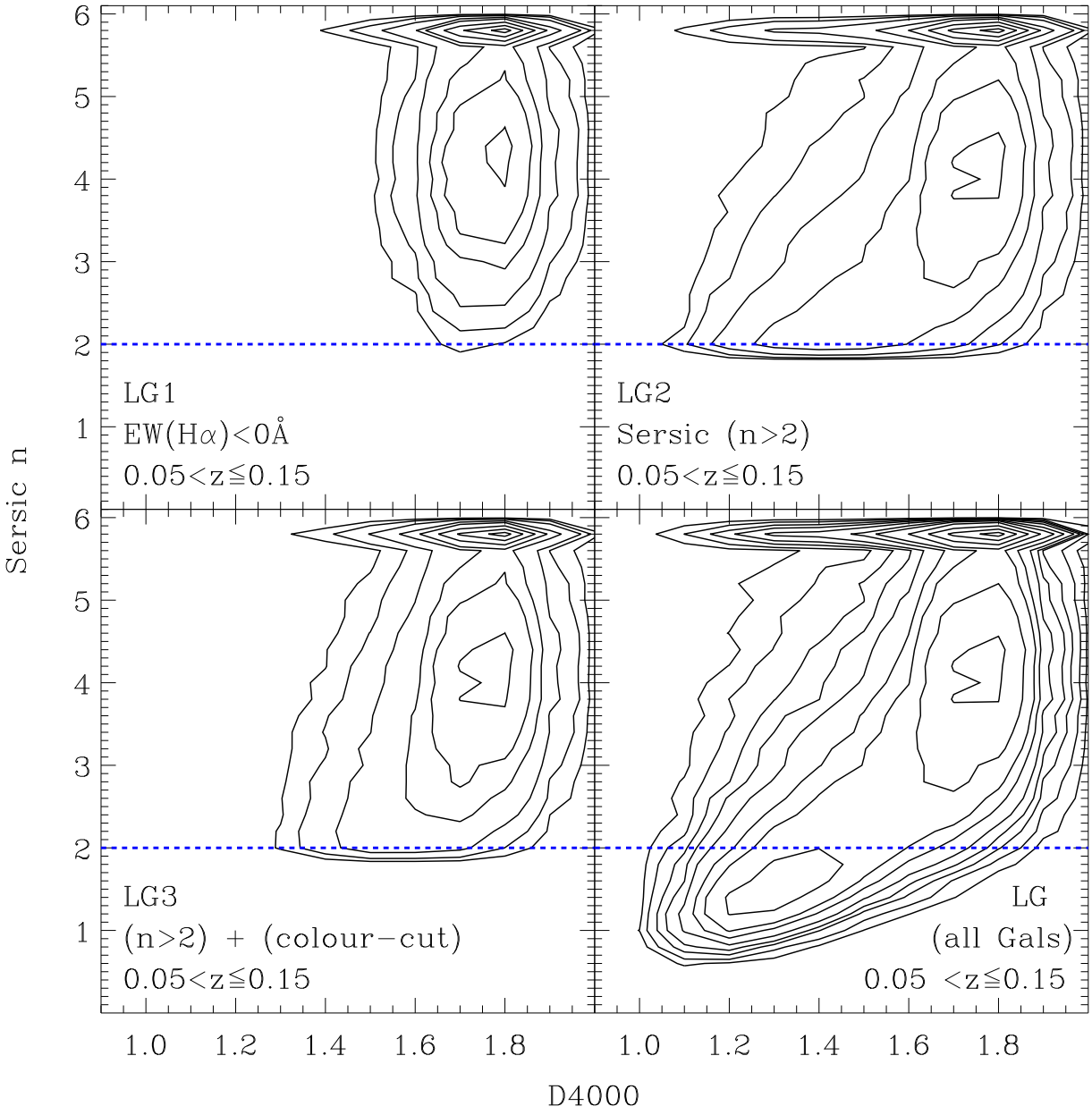

Figure 3.12: The Sérsic n vs. D4000 diagrams of the LG1 (upper left panel), LG2 (upper right), and LG3 (lower left) samples. All galaxies in the LG sample are plotted in the lower right panel of this Figure. The 4 diagrams are comparable with the plots shown in Figure 3.12. However, the diagrams are not identical because the higher luminosity limit in the Luminous Galaxy sample excludes fainter galaxies which tend to also be younger (D4000 < 1.0), therefore the LG1 - LG3 samples have narrower D4000 distributions (see also Figure 3.11) than the Main Galaxy samples (MG1, MG2, & MG3).

Chapter 4

Discussion

Different approaches are possible to identify the stellar old galaxies of the local Universe; the most common is to isolate the red sequence in colour-magnitude space, because it is known that stellar old galaxies account for the majority of red sequence objects. Unfortunately, the red sequence consists not only of red and old objects. Younger galaxies can also be located in the red sequence due to their high dust component. The dust inside these young and starforming galaxies reddens the emitted light. Therefore, the galaxy's colour is not a reliable indicator of age, because one has to know first how dusty the object of interest is.
One can exclude such younger & starforming objects from the red sequence by using galaxy morphology as a selection parameter. It is believed that the stellar age of galaxies and the object's morphology are correlated. In this spirit one thinks that younger galaxies feature late-type morphology and stellar older objects have early-type looks (Gallazzi *et al.* 2006 [25]).

4.1 Selecting by Sérsic index

We follow Hogg *et al.* 2004 [31] and use the Sérsic index $n > 2$ as selection parameter to isolate early-type objects from a complete galaxy sample of the local Universe (Section 2.2). This morphology selection based on Sérsic index n (MG2 sample) shows an in colour extended red sequence (Figure 3.1) with an average scatter of ~ 0.1 (σ_{MAD}-value). To find a reliable colour-magnitude relation (CMR) of this sample one has to apply a robust fitting method. Doing so we find a CMR slope of $\sim$ -0.02, that is consistent with the slope value of -0.022 found in the Sérsic-selected galaxy sample of Hogg *et al.* 2004 [31]. The sample's high scatter around its fitted CMR and the extended distribution of the MG2 colour residuals $\triangle(g' - r')$ in colour space (Figure 3.2) are due to the inclusion of blue galaxies; about 25% of the sample population are bluer than the red sequence lying below its colour limit ($3\sigma_{\mathrm{MAD}}$-limit of the Hα-selected red sequence).

Looking into the sample's average spectrum verifies the numerous inclusion of blue and star forming galaxies (Figure 3.3). Its flattened SED continuum and the strong emissions in Hα, Hβ, [OII], and [OIII] are explicit indicators of star forming and/or AGN objects located inside the Sérsic selected galaxy sample of MG2. BPT-diagnostics can help quantifying the sample's contamination of these active galaxies (Figure 3.4). The calculated fractions of starforming and/or AGN galaxies included in our MG2 sample decrease with z due to the redshift dependent luminosity limits in $M_{r'}$ (see Figure 2.1). However, not less than $\sim 13\%$ of the MG2 population are active galaxies featuring star formation and/or AGN activity (for $z < 0.15$). This fraction can rise up to more than 30% at low redshifts ($z < 0.06$).
The sample's contamination of blue and starforming objects is also visible in the D4000 histogram of the MG2 galaxies (Figure 3.5). The D4000-values of the MG2 members extend over a wide range spanning from 2.1 to 0.9. About 15% of the MG2 galaxies show a D4000-value less than 1.3. These objects are also responsible for lowering the D4000 mean of the MG2 sample to only $\sim$ 2.5 1.6. This low D4000 average is also visible in the sample's average spectrum (Figure 3.3's mid panel) there low elevated 4000Å-break has only a D4000 flux ratio of ~ 1.6, consistent with the sample's calculated D4000 mean. The D4000-value is a commonly used age estimator, using the stellar model synthesis code of Bruzual & Charlot 2003 [12] enable us to calculate the sample's average stellar age. The MG2 galaxies have on average a stellar age of ~ 2.5 Gyr. Due to the nature of the D4000 flux ratio, this age value is luminosity dependent.
Using higher luminosities limits in this Sérsic selection can reduce the sample's contamination of blue starforming young galaxies and therefore increase the sample's average stellar age (see Tables 3.4 & 3.10). Nevertheless, selecting by Sérsic n will still include numerous young galaxies, even in the case of luminous galaxies (see Figure 3.11). Repeating the age analysis on the high luminous galaxy sample (LG2) shows that the selection's mean stellar age is between 2.75 - 3.00 Gyr, an average age increase of about maximal 0.5 Gyr compared to the earlier found result of the on average lower luminous galaxy sample of MG2.
Based on the low average age of the Sérsic selections (MG2 & LG2) we conclude that the Sérsic criterion alone is not capable enough to identify non-star forming stellar old red sequence galaxies. It is unqualified for our purpose, since this morphology parameter features a too weak correlation with stellar age (see Figure 3.6) and star formation activity (see Figure 3.3). Furthermore, the Sérsic index n does not seem to correlate in general as well as needed with other galaxy parameters, like the galaxy's position on the red sequence or the spectral lines of Hα and O[II], typically used in the identification of aged objects. The Sérsic index n can therefore not be characterised as a robust, effective and reliable age separator of galaxies. It should be also noted here that it becomes more difficult to measure surface brightness profiles of galaxies at higher redshifts ($z > 2$) due to the fixed resolution of telescopes. Therefore, it is unlikely to calculate Sérsic indices correctly at higher z. Thus, we conclude that the Sérsic index n is not a reliable criterion to identify high redshift early-type

red sequence galaxies.

4.2 Selecting by Sérsic index & Colour

To verify the impact of additional colour information we decide to select not only by Sérsic n but also by colour $(g' - r')$. Excluding bluer early-type galaxies by applying a colour-cut inside the Sérsic selection reduces the number of sample galaxies about $\sim 25\%$. The resulting galaxy selection (MG3) forms a tight red sequence (Figure 3.1) with less scatter ($\sigma_{\mathrm{MAD}} \sim 0.6$) than the pure Sérsic selected sample (MG2), therefore th MG3 sample shows a much stronger CMR than the MG2 sample. However, the CMR of MG3 is identical with the CMR of MG2.

The MG3 sample features a smaller fraction of starforming ($\sim 0.7\%$) and AGN/starforming ($\sim 3.5\%$) galaxies (Figure 3.4) than MG2. The AGN fraction of MG3 ($\sim 3\%$) is also half the size of the MG2 AGN fraction. AGN & AGN/starforming galaxies are mostly responsible for the net line emissions detectable in MG3 (see Figures 3.3 & 3.4). The sample's average spectrum shows an explicitly early-type shaped continnum (SED) and features a clear absorption in Hβ. The D4000 flux ratio of this average spectrum is with 1.70 higher than in MG2 and counts for an elevated 4000Å-break. It indicates also that the MG3 sample is mainly populated by stellar old galaxies. An indeed, the MG3 fraction of young galaxies is samller than that of MG2, because that sample does not contain the stellar youngest early-type galaxies of MG2 (Figures 3.5 & 3.6). This results in a higher D4000 mean and in a higher average age of ~ 3.0 Gyr. The MG3 sample is on average about 0.5 Gyr older than the pure Sérsic selected sample of MG2.

One can increase the average stellar age of the MG3 sample by maximal 0.5 Gyr using higher luminosities as additional selection criteria (see Tables 3.6, 3.7 & 3.10). The age gap between the Sérsic selections (MG2 & LG2) and the Sérsic & colour selected samples (MG3 & LG3) on the other hand is on average independent of the used luminosity limits and remains with ~ 0.5 Gyr constant in redshift space ($z \leq 0.15$). Higher luminosity limits ($M_{r'}$-cuts) reduce also the sample's contamination of young starforming galaxies but cannot prevent the inclusion of AGN objects (see Tables 3.5 & 3.9).

The combined criteria of Sérsic n & colour have improved our search for stellar old galaxies of the local Universe, but show also weaknesses. The combined information of morphology (Sérsic n) and colour $(g' - r')$ are capable of constructing a reliable red sequence sample, but cannot exclude strictly enough stellar younger objects and AGN or AGN/starforming galaxies from contaminating the sample. Therefore we conclude that these 2 criteria correlate to weak with the stellar age of galaxies. As mentioned earlier, it is difficult to measure Sérsic indices correctly at high redshifts due to the fixed resolution of telescopes. Therefore, selecting stellar old early-type galaxies by Sérsic n & colour is not reliable at high z.

4.3 Selecting by Hα

We can select stellar old early-type galaxies more effectively by changing from photometric selection criteria to only one single spectroscopic criterion: the EW of Hα. Looking only at Hα-absorbers (MG1) results in a very tight red sequence with the lowest scatter ($\sigma_{\mathrm{MAD}} \sim 0.5$) of all 3 analysed galaxy samples (Figures 3.2 & 3.1). The CMR of this red sequence has a slope of $\sim$ -0.02. Thus, the CMR slopes of all 3 samples (MG1, MG2 & MG3) are consistent with each other, although the 3 red sequence samples look differently in CM-space.
For identifying stellar old early-type red sequence galaxies the single Hα-criterion is the strictest and most efficient selection parameter. Neither starforming nor AGN galaxies are included in the Hα-selection since we demand that all sample members have an EW(Hα) < 0Å. The precise exclusion of active galaxies results in a total passive average spectrum where no indication of any ongoing star formation or AGN activity is detected (Figure 3.3). The Hα-sample's average spectrum shows the highest 4000Å-break (D4000 ~ 1.76) and the deepest absorption features of all sample spectra. It is also the only sample spectrum where Hα, Hβ, [OII], and [OIII] are simultaneously in clear absorption.
The Hα-sample is the only galaxy selection in which no younger galaxies are inclosed (D4000 < 1.3; see Figures 3.5 & 3.6). It is the only sample showing a symmetric distribution in D4000 space. This sample features also with ~ 1.77 the highest D4000 mean. It is the most uniform aged galaxy sample and has therefore also the highest average stellar age ($\sim$ 4Gyr) of all here presented galaxy samples.
Like mentioned earlier, it is possible to increase the sample's average stellar age by ~ 0.5 Gyr if one uses higher luminosity limits (see Tables 3.6, 3.7 & 3.10). The age gap between the different galaxy selections (MG1, MG2 & MG3) remains nearly constant if one uses consistent $M_{r'}$-cuts inside the samples. The Hα-sample (MG1) is on average about 0.75 - 1.0 Gyr older than the Sérsic n & colour selected sample (MG3). The age difference between the Hα-sample and the pure Sérsic selected sample (MG2) is with ~ 1.5 Gyr even more higher.
We have seen that our Hα-criterion correlates much stronger with stellar age than the photometric parameters of morphology (Sérsic n) and colour ($g' - r'$). We have also seen that the Hα-absorption correlates strong with the galaxy's morphology parameter of Sérsic index n. Our Hα-sample consist nearly exclusively of early-type galaxies independent of the used luminosity limits or redshifts (Sérsic $n > 2$; see upper left panels of Figure 3.6 & 3.12). It is therefore the best selection criterion to identify old early-type red sequence galaxies at high z.

Chapter 5

Conclusion

The Hα-absorption is the best and most reliable indicator to isolate redshift independently stellar old galaxies of the red sequence. We have shown that the single Hα-criterion correlates strongly with galaxy colour ($g' - r'$), morphology (Sérsic index n), star formation activity, stellar age and other spectral indices (4000Å-break, O[II]-line) typically used in the identification and characterisation of stellar old galaxies. The parameters of Sérsic n and/or galaxy colour show only a weak correlation with the stellar age of galaxies: Not every early-type galaxy is a non-star forming red system of older age, but every Hα-absorber is a red non-star forming stellar old galaxy with at least minor early-type morphology (Sérsic $n \geq 2$). By using Hα-absorption (spectroscopy) we can identify early-type galaxies directly and this even at redshifts where ground based telescopes do not have the ability to resolve galaxy morphology photometricly (fixed maximal telescope resolution).
Using our Hα-absorption criterion at high redshifts ($z > 2$) should enable us to observe when the first Hα-passive systems appeared and when they joined the red sequence. Having detectable Hα-absorbers we can then follow our tight red sequence of Hα-passive early-type galaxies through redshift space & time. This would enable us to observe the evolutionary changes of the red sequence in more detailed way than before (evolution of the CMR). We could follow the built-up of the red sequence and determine which formation scenario of early-type galaxy is most likely responsible for the mass assembly of the red sequence. We would also get new insights about how stellar old passive galaxies affect the colour-magnitude relation with time.
Taking into account that the most massive & luminous early-type galaxies are also the stellar oldest ones, and knowing that these galaxies are located inside hot and dense cluster environments, one could use the Hα-absorption criterion to identify the most luminous & oldest Hα-absorbers at many redshifts. This information could then be used to follow the evolution of the Universe's most dense regions by tracing the most luminous & oldest Hα-absorbers through redshift space.

Bibliography

[1] J. K. Adelman-McCarthy, M. A. Agüeros, S. S. Allam, C. Allende Prieto, K. S. J. Anderson, and *et al.* "The Sixth Data Release of the Sloan Digital Sky Survey". *Astrophysical Journal Letters*, 175:297–313, April 2008.

[2] J. A. Baldwin, M. M. Phillips, and R. Terlevich. "Classification parameters for the emission-line spectra of extragalactic objects". *Astronomical Society of the Pacific*, 93:5–19, February 1981.

[3] W. A. Baum. "The Hertzsprung-Russell diagrams of old stellar Populations". In J. L. Greenstein, editor, *The Hertzsprung-Russell Diagram*, volume 10 of *IAU Symposium*, pages 23–+, 1959.

[4] E. F. Bell, C. Wolf, K. Meisenheimer, H.-W. Rix, A. Borch, S. Dye, M. Kleinheinrich, L. Wisotzki, and D. H. McIntosh. "Nearly 5000 Distant Early-Type Galaxies in COMBO-17: A Red Sequence and Its Evolution since z˜1". *Astrophysical Journal*, 608:752–767, June 2004.

[5] M. R. Blanton, D. Eisenstein, D. W. Hogg, D. J. Schlegel, and J. Brinkmann. "Relationship between Environment and the Broadband Optical Properties of Galaxies in the Sloan Digital Sky Survey". *Astrophysical Journal*, 629:143–157, August 2005.

[6] M. R. Blanton and S. Roweis. "K-Corrections and Filter Transformations in the Ultraviolet, Optical, and Near-Infrared". *Astronomical Journal*, 133:734–754, February 2007.

[7] M. R. Blanton, D. J. Schlegel, M. A. Strauss, J. Brinkmann, D. Finkbeiner, and *et al.* "New York University Value-Added Galaxy Catalog: A Galaxy Catalog Based on New Public Surveys". *Astronomical Journal*, 129:2562–2578, June 2005.

[8] R. G. Bower, A. J. Benson, R. Malbon, J. C. Helly, C. S. Frenk, C. M. Baugh, S. Cole, and C. G. Lacey. "Breaking the hierarchy of galaxy formation". *Monthly Notices of the Royal Astronomical Society*, 370:645–655, August 2006.

[9] R. G. Bower, J. R. Lucey, and R. S. Ellis. "Precision Photometry of Early Type Galaxies in the Coma and Virgo Clusters - a Test of the Universality of the Colour / Magnitude Relation - Part Two - Analysis". *Monthly Notices of the Royal Astronomical Society*, 254:601–+, February 1992.

[10] R. G. Bower, J. R. Lucey, and R. S. Ellis. "Precision photometry of early-type galaxies in the Coma and Virgo clusters: A test of the universality of the colour-magnitude relation. I - The data. II. Analysis". *Monthly Notices of the Royal Astronomical Society*, 254:589–613, February 1992.

[11] G. Bruzual. "Spectral evolution of galaxies. I - Early-type systems". *Astrophysical Journal*, 273:105–127, October 1983.

[12] G. Bruzual and S. Charlot. "Stellar population synthesis at the resolution of 2003". *Monthly Notice of the Royal Astronomical Society*, 344:1000–1028, October 2003.

[13] G. Bruzual A. "Spectral evolution of galaxies. I - Early-type systems". *Astrophysical Journal, Part 1*, Vol. 273:105–127, October 1983.

[14] D. J. Croton, V. Springel, S. D. M. White, G. De Lucia, C. S. Frenk, L. Gao, A. Jenkins, G. Kauffmann, J. F. Navarro, and N. Yoshida. "Erratum: The many lives of active galactic nuclei: cooling flows, black holes and the luminosities and colours of galaxies". *Monthly Notices of the Royal Astronomical Society*, 367:864–864, April 2006.

[15] G. de Vaucouleurs. "Recherches sur les nébuleuses extragalactiques". *Journal des Observateurs*, 31:113–+, January 1948.

[16] K. Degiola-Eastwood and G. L. Grasdalen. "The range of V - R colors for a cluster of E and S0 galaxies as a function of redshift". *Astrophysical Journal Letters*, 239:L1–L3, July 1980.

[17] A. Dressler and J. E. Gunn. "Spectroscopy of galaxies in distant clusters. II - The population of the 3C 295 cluster". *Astrophysical Journal*, 270:7–19, July 1983.

[18] R. S. Ellis, I. Smail, A. Dressler, W. J. Couch, A. J. Oemler, H. Butcher, and R. M. Sharples. "The Homogeneity of Spheroidal Populations in Distant Clusters". *Astrophysical Journal*, 483:582–+, July 1997.

[19] S. M. Faber. "Variations in Spectral-Energy Distributions and Absorption-Line Strengths among Elliptical Galaxies". *Astrophysical Journal*, 179:731–754, February 1973.

[20] S. M. Faber, S. C. Trager, J. J. Gonzalez, and G. Worthey. "The Stellar Ages of Elliptical Galaxies". In P. C. van der Kruit and G. Gilmore, editors, *Stellar Populations*, volume 164 of *IAU Symposium*, pages 249–+, 1995.

[21] I. Ferreras, S. Charlot, and J. Silk. "The Age and Metallicity Range of Early-Type Galaxies in Clusters". *Astrophysical Journal*, 521:81–89, August 1999.

[22] G. Feulner, Y. Goranova, N. Drory, U. Hopp, and R. Bender. "The connection between star formation and stellar mass: specific star formation rates to redshift one". *Monthly Notices of the Royal Astronomical Society*, 358:L1–L5, March 2005.

[23] G. Feulner, U. Hopp, and C. S. Botzler. "Integrated specific star formation rates of galaxies, groups, and clusters: a continuous upper limit with stellar mass?". *Astronomy and Astrophysics*, 451:L13–L16, May 2006.

[24] M. Fukugita, T. Ichikawa, J. E. Gunn, M. Doi, K. Shimasaku, and D. P. Schneider. "The Sloan Digital Sky Survey Photometric System". *Astronomical Journal*, 111:1748–+, April 1996.

[25] A. Gallazzi, S. Charlot, J. Brinchmann, and S. D. M. White. "Ages and metallicities of early-type galaxies in the Sloan Digital Sky Survey: new insight into the physical origin of the colour-magnitude and the $Mg_2 - \sigma_V$ relations". *Monthly Notice of the Royal Astronomical Society*, 370:1106–1124, August 2006.

[26] R. M. González Delgado, M. Cerviño, L. P. Martins, C. Leitherer, and P. H. Hauschildt. "Evolutionary stellar population synthesis at high spectral resolution: optical wavelengths". *Monthly Notices of the Royal Astronomical Society*, 357:945–960, March 2005.

[27] G. J. Graves, S. M. Faber, and R. P. Schiavon. "Dissecting the Red Sequence. I. Star-Formation Histories of Quiescent Galaxies: The Color-Magnitude versus the Color-σ Relation". *Astrophysical Journal*, 693:486–506, March 2009.

[28] G. J. Graves, S. M. Faber, R. P. Schiavon, and R. Yan. "Ages and Abundances of Red Sequence Galaxies as a Function of LINER Emission-Line Strength". *Astrophysical Journal*, 671:243–271, December 2007.

[29] J. E. Gunn, M. Carr, C. Rockosi, M. Sekiguchi, K. Berry, and *et al.* "The Sloan Digital Sky Survey Photometric Camera". *Astronomical Journal*, 116:3040–3081, December 1998.

[30] D. W. Hogg, I. K. Baldry, M. R. Blanton, and D. J. Eisenstein. "The K correction". *ArXiv Astrophysics e-prints*, October 2002.

[31] D. W. Hogg, M. R. Blanton, J. Brinchmann, D. J. Eisenstein, D. J. Schlegel, and *et al.* "The Dependence on Environment of the Color-Magnitude Relation of Galaxies". *Astrophysical Journal Letters*, 601:L29–L32, January 2004.

[32] R. A. Jansen, M. Franx, and D. Fabricant. "[O II] As a Tracer of Current Star Formation". *Astrophysical Journal*, 551:825–832, April 2001.

[33] G. Kauffmann and S. Charlot. "Chemical enrichment and the origin of the colour-magnitude relation of elliptical galaxies in a hierarchical merger model". *Monthly Notices of the Royal Astronomical Society*, 294:705–+, March 1998.

[34] G. Kauffmann, T. M. Heckman, C. Tremonti, J. Brinchmann, S. Charlot, and *et al.* "The host galaxies of active galactic nuclei". *Monthly Notice of the Royal Astronomical Society*, 346:1055–1077, December 2003.

[35] G. Kauffmann, T. M. Heckman, S. D. M. White, S. Charlot, C. Tremonti, and et al. "Stellar masses and star formation histories for 10^5 galaxies from the Sloan Digital Sky Survey". *Monthly Notice of the Royal Astronomical Society*, Vol. 341:33–53, May 2003.

[36] G. Kauffmann, T. M. Heckman, S. D. M. White, S. Charlot, C. Tremonti, and *et al.* "Stellar masses and star formation histories for 10^5 galaxies from the Sloan Digital Sky Survey". *Monthly Notices of the Royal Astronomical Society*, 341:33–53, May 2003.

[37] R. C. Kennicutt, Jr. "Star Formation in Galaxies Along the Hubble Sequence". *Annual Review of Astronomy and Astrophysics*, 36:189–232, 1998.

[38] L. J. Kewley, M. A. Dopita, R. S. Sutherland, C. A. Heisler, and J. Trevena. "Theoretical Modeling of Starburst Galaxies". *Astrophysical Journal*, 556:121–140, July 2001.

[39] P. Merluzzi, G. Busarello, M. Massarotti, and F. La Barbera. "The Colour-Magnitude Relation and the Age of Galaxies in the Cluster AC118 at z=0.31". In S. Borgani, M. Mezzetti, and R. Valdarnini, editors, *Tracing Cosmic Evolution with Galaxy Clusters*, volume 268 of *Astronomical Society of the Pacific Conference Series*, pages 413–+, 2002.

[40] R. G. Miller. "The Jackknife - a Review". *biometrika*, 61(1):1–15, April 1974.

[41] J. Moustakas, R. C. Kennicutt, Jr., and C. A. Tremonti. "Optical Star Formation Rate Indicators". *Astrophysical Journal*, 642:775–796, May 2006.

[42] A. D. Quintero, D. W. Hogg, M. R. Blanton, D. J. Schlegel, and D. J. *et al.* Eisenstein. "Selection and Photometric Properties of K+A Galaxies". *Astrophysical Journal*, 602:190–199, February 2004.

[43] A. Sandage. *"The Hubble atlas of galaxies"*. 1961.

[44] A. Sandage and N. Visvanathan. "The color-absolute magnitude relation for E and S0 galaxies. II - New colors, magnitudes, and types for 405 galaxies". *Astrophysical Journal*, 223:707–729, August 1978.

[45] D. J. Schlegel, D. P. Finkbeiner, and M. Davis. "Maps of Dust Infrared Emission for Use in Estimation of Reddening and Cosmic Microwave Background Radiation Foregrounds". *Astrophysical Journal*, 500:525–+, June 1998.

[46] J. L. Sérsic. "Influence of the atmospheric and instrumental dispersion on the brightness distribution in a galaxy". *Boletin de la Asociacion Argentina de Astronomia La Plata Argentina*, 6:41–+, 1963.

[47] J. L. Sersic. *"Atlas de galaxias australes"*. Cordoba, Argentina: Observatorio Astronomico, 1968, 1968.

[48] C. Stoughton, R. H. Lupton, M. Bernardi, M. R. Blanton, S. Burles, and *et al.* "Sloan Digital Sky Survey: Early Data Release". *Astronomical Journal*, 123:485–548, January 2002.

[49] M. A. Strauss, D. H. Weinberg, R. H. Lupton, V. K. Narayanan, J. Annis, and *et al.* "Spectroscopic Target Selection in the Sloan Digital Sky Survey: The Main Galaxy Sample". *Astronomical Journal*, 124:1810–1824, September 2002.

[50] D. Thomas, C. Maraston, R. Bender, and C. Mendes de Oliveira. "The Epochs of Early-Type Galaxy Formation as a Function of Environment". *Astrophysical Journal*, 621:673–694, March 2005.

[51] N. Visvanathan and A. Sandage. "The color-absolute magnitude relation for E and S0 galaxies. I - Calibration and tests for universality using Virgo and eight other nearby clusters". *Astrophysical Journal*, 216:214–226, August 1977.

[52] S. M. Weinmann, F. C. van den Bosch, X. Yang, and H. J. Mo. "Properties of galaxy groups in the Sloan Digital Sky Survey - I. The dependence of colour, star formation and morphology on halo mass". *Monthly Notices of the Royal Astronomical Society*, 366:2–28, February 2006.

[53] G. Worthey. "Comprehensive stellar population models and the disentanglement of age and metallicity effects". *Astrophysical Journal Supplement Series*, 95:107–149, November 1994.

[54] L. Yan, D. Thompson, and B. T. Soifer. "Optical Spectroscopy of K-Selected Extremely Red Galaxies". *The Astronomical Journal*, 127:1274–1284, March 2004.

[55] R. Yan, J. A. Newman, S. M. Faber, N. Konidaris, D. Koo, and M. Davis. "On the Origin of [O II] Emission in Red-Sequence and Poststarburst Galaxies". *Astrophysical Journal*, 648:281–298, September 2006.

[56] D. G. York, J. Adelman, J. E. Anderson, Jr., S. F. Anderson, J. Annis, and *et al.* "The Sloan Digital Sky Survey: Technical Summary". *Astronomical Journal*, 120:1579–1587, September 2000.